THE BELL SYSTEM TECHNICAL JOURNAL
Vol. 50, No. 3, March, 1971
Printed in U.S.A.

Device Implications of the Theory of Cylindrical Magnetic Domains*

By A. A. THIELE

(Manuscript received October 7, 1970)

This paper applies the theory of cylindrical magnetic domains[1] to cylindrical domain devices. The stability conditions are examined as bounds to the region of possible device operation and it is found that the plate thickness, $h = 4l$, and the domain diameter, $d = 8l$, where l is the ratio of the wall energy per unit area to 4π times the saturation magnetization squared, are preferred values. When the effects of wall coercivity and mobility are examined, it is found that the preferred plate thickness and domain diameter are even more strongly preferred, that the wall motion coercivity should be less than one percent of 4π times the saturation magnetization, and that a domain coercivity and mobility may be defined. Consideration of the Néel temperature and the desired absolute domain size in addition to the static stability conditions shows that domain materials having some antiferromagnetic character and induced uniaxial anisotropy are preferred. Where appropriate, domain methods for measuring material parameters are described.

I. INTRODUCTION

The application of cylindrical magnetic domains or "bubbles" to memory and logic devices has recently received considerable attention.[2-6] Such domain devices may operate in a continuum of modes ranging from the wall motion coercivity dominated mode to the "hard bubble" mode. In the coercivity dominated mode, applied fields determine the domain configuration which is then maintained by coercivity. In the hard bubble mode the coercivity must be sufficiently low that the domains have a well-defined size and shape permitting the move-

* Portions of this article were presented at the "Fifteenth Annual Conference on Magnetism and Magnetic Materials" Philadelphia, Pennsylvania, on Nov. 20, 1969. (See Ref. 2.)

ment of individual domains as distinct entities. A previous paper developed the theory of static stability of cylindrical domains in materials having zero coercivity.[1] The present work applies this theory to the determination of the preferred conditions for construction of devices operating in the hard bubble mode. It is found that specifying an operating domain diameter determines preferred values for the plate thickness, magnetization, anisotropy constant and the maximum allowable value of the wall motion coercivity.

Figure 1 shows the model for the domain structure from which the static stability theory was developed. The coordinate system and symbols used here are the same as in Ref. 1 except for the addition of a few symbols such as μ_w, the wall mobility; H_c, the wall motion coercivity; $\mathbf{v}_d$, the domain velocity; and $\Delta\sigma_w$ the variation in wall energy. The model represents a single isolated domain in a plate of magnetic material of uniform thickness, h, and an infinite extent in the plane, $r_f = \infty$. Everywhere within the material the magnetization has a uniform (saturation) magnitude, M_s, directed along the upward plate normal (the z direction) within the domain and along the downward plate normal elsewhere within the material. The domain wall is assumed to have negligible width and the domain wall energy density, σ_w, is initially taken to be independent of both wall orientation and curvature. The domain wall is cylindrical in the sense that it everywhere contains a line parallel to the plate normal. Under these assump-

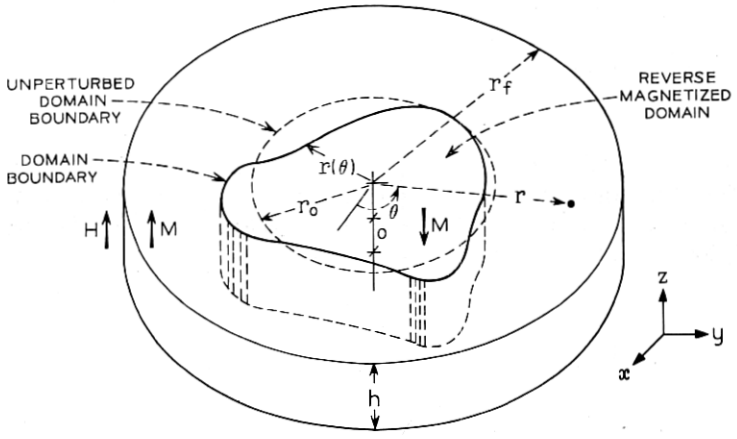

Fig. 1—Domain configuration and coordinate system.

tions only the component of the spatially uniform applied field which lies along the plate normal will interact with the domain so that only this component is considered. This component is denoted by H and is taken positive when directed upward, the direction tending to collapse the domain.

The assumptions implicit in this domain model are not all independent. The interrelation of the assumptions and the dependence of the assumptions on the domain geometry and the material parameters are discussed on pp. 3312–3318 of Ref. 1. The validity of the assumptions will not be discussed further here except to note that in order for domains of the type to be considered here to exist, domain nucleation and wall-width considerations require roughly that

$$K_u > 2\pi M_s^2 , \tag{1}$$

where K_u is the uniaxial anisotropy constant, and that the validity of the approximations generally improves as K_u is increased above this minimum value.

The domain radius function, $r_b(\theta)$, which is expanded in the series

$$r_b(\theta) = r_0 + \Delta r_0 + \sum_{n=1}^{\infty} \Delta r_n \cos [n(\theta - \theta_n - \Delta\theta_n)], \tag{2}$$

describes the domain shape in the plane. The Δr_n and $\Delta\theta_n$ describe a variation in domain size and shape from a circular domain of radius $r_b(\theta) = r_0$ and the θ_n describe the direction of the variation. (The $\Delta\theta_n$ have significance only for second variations.) Since only near circular domains are of interest here, the condition

$$|r_0| \gg |\Delta r_0| + \sum_{n=1}^{\infty} n\, |\Delta r_n| \tag{3}$$

is imposed to assure that the radius is single valued and smooth.

The first and second variations of the total domain energy with respect to the Δr_n and $\Delta\theta_n$ determine the domain equilibrium and stability conditions. The total domain energy,

$$E_T = E_W + E_H + E_M, \tag{4}$$

is the sum of three terms. The wall energy, E_W, is the product of the wall energy density and the wall area. The applied field interaction energy, E_H, is proportional to the product of the domain volume and the external field interaction energy. The last term, E_M, is the internal magnetostatic energy of the domain. The energy variation has the

form

$$\Delta E_T = \sum_{n=0}^{\infty} \left[\left(\frac{\partial E_T}{\partial r_n} \right)_0 \Delta r_n + \left(\frac{\partial E_T}{\partial \theta_n} \right)_0 \Delta \theta_n \right] + \frac{1}{2} \sum_{n=0}^{\infty} \sum_{m=0}^{\infty} \left[\left(\frac{\partial^2 E_T}{\partial r_n \, \partial r_m} \right)_0 \Delta r_n \, \Delta r_m + 2 \left(\frac{\partial^2 E_T}{\partial r_n \, \partial \theta_m} \right)_0 \Delta r_n \, \Delta \theta_m + \left(\frac{\partial^2 E_T}{\partial \theta_n \, \partial \theta_m} \right)_0 \Delta \theta_n \, \Delta \theta_m \right] + O_3 \tag{5}$$

where in the energy derivatives the independent variables, the Δr_n and $\Delta \theta_n$, have been written as r_n and θ_n for compactness, the zero subscript indicates that the derivatives are to be evaluated for a strictly circular domain, $r_b(\theta) = r_0$, and O_3 indicates terms of order three or higher. The first derivatives are the negative of the generalized forces, $-(\partial E_T/\partial r_n)_0$ and $-(\partial E_T/\partial \theta_n)_0$ being respectively the radial and angular generalized forces of rotational periodicity n. The second derivatives form the stiffness matrix of the system with $(\partial^2 E_T/\partial r_n \, \partial r_m)_0$ being the (n, m) element of the radial submatrix and $(\partial^2 E_T/\partial r_n \, \partial \theta_m)_0$ and $(\partial^2 E_T/\partial \theta_n \, \partial \theta_m)_0$ being the corresponding elements of the mixed and angular submatrices respectively. In Ref. 1 the derivatives of the total energy with respect to the Δr_n and $\Delta \theta_n$ were obtained by differentiating the integrals which form the terms of equation (4) and evaluating the resulting integrals for the case of a strictly circular domain.

In the present work it is convenient to write the energy variation expression in a normalized form in which: energy is measured in units of $4(2\pi M_s^2)(\pi h^3)$, the equilibrium condition has been used to eliminate the applied field from the second variations (the stiffness matrix is of interest here only for a domain in equilibrium), the first- and second-order variations which are identically zero and deleted, and the nonzero generalized forces and stiffness matrix elements are written as functions of dimensionless variables, the applied field measured in units of the magnetization, $H/4\pi M_s$, and ratios of the plate thickness, h, the domain diameter, $d = 2r_0$, and the characteristic length of the material,

$$l = \sigma_w / 4\pi M_s^2 . \tag{6}$$

This normal form of the energy variation is [Ref. 1, equation (68)]

$$\frac{\Delta E_T}{4(2\pi M_s^2)(\pi h^3)} = \left[\frac{l}{h} + \frac{d}{h} \frac{H}{4\pi M_s} - F\left(\frac{d}{h}\right) \right] \frac{\Delta r_0}{h}$$

$$+\frac{1}{2}\left\{-\left(2\frac{h}{d}\right)\left[\frac{l}{h}-S_0\left(\frac{d}{h}\right)\right]\left(\frac{\Delta r_0}{h}\right)^2 + \sum_{n=2}^{\infty}(n^2-1)\left(\frac{h}{d}\right)\left[\frac{l}{h}-S_n\left(\frac{d}{h}\right)\right]\left(\frac{\Delta r_n}{h}\right)^2\right\}+O_3 \quad (7)$$

where F and the S_n are called the force and stability functions respectively and are written in terms of the complete elliptic integral of the first kind,

$$K(m) \equiv \int_0^{\pi/2}(1-m\sin^2\theta)^{-\frac{1}{2}}\,d\theta, \quad (8)$$

the complete elliptic integral of the second kind,

$$E(m) \equiv \int_0^{\pi/2}(1-m\sin^2\theta)^{\frac{1}{2}}\,d\theta \quad (9)$$

and the L_n functions which are auxiliary functions introduced for convenience,

$$L_0(x) = 0 \quad (10a)$$

$$L_1(x) = 4[(x+1)^{\frac{1}{2}}E((1+x)^{-1}) - x(x+1)^{-\frac{1}{2}}K((1+x)^{-1})] \quad (10b)$$

$$L_{n+1}(x) = \frac{1}{2n+1}[4n(2x+1)L_n(x) - (2n-1)L_{n-1}(x) - 16nx(x+1)^{-\frac{1}{2}} \times K((1+x)^{-1})], \quad n \geqq 1. \quad (10c)$$

The force and stability functions are

$$F(x) = \frac{2}{\pi}x^2[(1+x^{-2})^{\frac{1}{2}}E((1+x^{-2})^{-1}) - 1], \quad (11)$$

$$S_0(x) = F(x) - x\frac{\partial}{\partial x}F(x), \quad (12a)$$

$$= -\frac{1}{2\pi}x^2[L_1(x^{-2}) - L_1(0)], \quad (12b)$$

and

$$S_n(x) = -\frac{1}{n^2-1}\frac{1}{2\pi}x^2[L_n(x^{-2}) - L_1(x^{-2}) - L_n(0) + L_1(0)], \quad n \geqq 2. \quad (13)$$

Figure 3 of Ref. 1 plots $F(d/h)$ and $S_n(d/h)$ for $d/h \leqq 6$ and $n \leqq 10$.

Appendices A and B of Ref. 1 give methods of computation and series expansions of these functions while Section IV discusses the physical interpretation of the terms in the energy variation expansion [equation (5) here].

Section II of this paper discusses the domain size and stability implications of the energy variation expansion (7). This discussion yields the conditions for the existence of cylindrical domains in the total absence of dissipative processes and these existence conditions in turn place several restrictions upon device design. The section concludes with a discussion of domain size and domain ellipticity in the presence of anisotropic wall energy. Section III considers the effects of dissipative processes (wall motion coercivity and mobility) on domain existence and movement, the relation of domain mobility to wall mobility, and the limiting conditions under which the hard bubble mode may be achieved. Section IV combines the results obtained here and in Ref. 1 to obtain several relations between material parameters and device performance.

II. CYLINDRICAL DOMAIN SIZE, SHAPE AND STABILITY AT EQUILIBRIUM

This section examines the domain equilibrium and stability conditions and some of their implications.

2.1 *The Equilibrium Condition*

The domain is in equilibrium when all of the first-order variations of the total energy with respect to the Δr_n and $\Delta\theta_n$ are zero. In the variation expansion (7), all the first-order energy variations except the variation with respect to Δr_0 (representing a variation in domain size with no variation in shape) are identically zero. Since the domain is initially assumed to be a circular cylinder and there are no forces tending to deform it, the domain is in equilibrium when it is a circular cylinder having a diameter which is a solution to the normalized force equation,

$$\frac{l}{h} + \frac{d}{h}\frac{H}{4\pi M_s} - F\left(\frac{d}{h}\right) = 0. \tag{14}$$

The (normalized) generalized forces appearing in this equation have a one to one correspondence with the terms of the energy sum (4): the first term being produced by the wall energy, the second by the applied field, and the third by the internal magnetostatic energy. The normalized wall force, $-l/h = -\sigma_w/4\pi M_s^2 h$ always tends to collapse

the domain (σ_w and h are positive) and is independent of domain diameter. Each of the normalized generalized forces may be converted to an equivalent field by multiplying by $h4\pi M_s/d$. The equivalent wall field is $\sigma_w/2r_0M_s$ so that the wall field is proportional to the product of the wall energy and the wall curvature. The normalized applied field force, $-(d/h)(H/4\pi M_s)$, tends to collapse the domain for positive applied fields and its magnitude is proportional to the domain diameter. In this case the equivalent field is the applied field, H. The normalized internal magnetostatic force is $+F(d/h)$. The force function, F, is positive with positive first derivative and negative second derivative at all points. It approaches d/h for small domain diameters and $\pi^{-1} \ln | 4e^{\frac{1}{2}}d/h |$ for large domain diameters (In Ref. 1 see equation (138) and Fig. 3). Since F is positive, the internal magnetostatic force always tends to expand the domain. The internal magnetostatic force and the wall force are thus oppositely directed. Therefore equilibrium is attained for any given diameter by adjusting the applied field to a value which compensates for the difference in magnitude of these two forces, the sign of the field depending on which force is dominant. The equivalent field for the case of the internal magnetostatic force, $4\pi M_s \cdot (h/d)F(d/h)$, is the z averaged z component of the internal demagnetizing field or the internal magnetostatic scalar potential difference between the top and the bottom of the plate divided by the plate thickness.[1] This field approaches $4\pi M_s$ for small domain diameters and $4M_s(h/d) \ln | 4e^{\frac{1}{2}}d/h |$ for large domain diameters.

Solutions to the equilibrium problem may be discussed either in terms of the equivalent fields as was done by A. H. Bobeck[3] or in terms of the generalized force equation (14) with the preferred method depending on the specific application. In the present case, the generalized force equation will be used since the general properties of the solutions of the equilibrium problem may be easily obtained by straight line constructions on a plot of F.

Figure 2 shows examples of such constructions (along with stability constructions which will be explained later). The equilibrium construction consists of first locating the point on the vertical axis whose ordinate is l/h, then drawing a straight line through this point whose numerical slope is $H/4\pi M_s$. The line so constructed thus represents the first two terms in equation (14) so that its intersections with F (if any) are the equilibrium points. The dashed line asymptotic to the force function at the origin has numerical slope one and therefore provides a reference for estimating the magnitude of applied fields. In each of the constructions of Fig. 2, l/h is 0.3 and this point on the vertical axis is

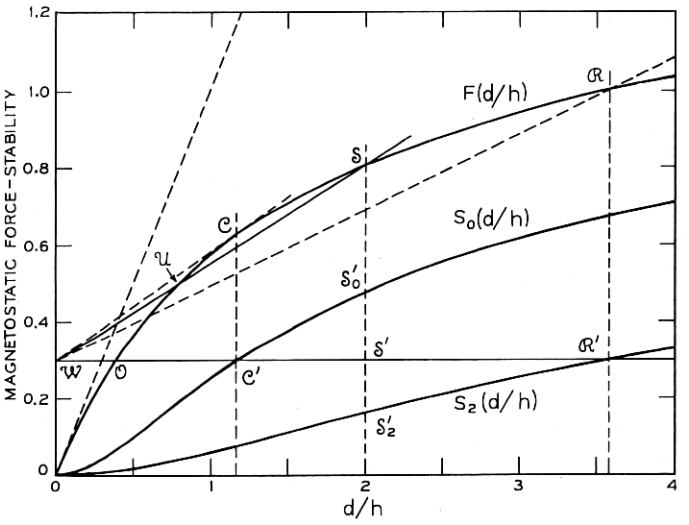

Fig. 2—Construction of solutions to the force equation for $l/h = 0.3$, $d = d_0$, $d = d_2$ and $d = 2h$.

denoted by $\mathfrak{W}$. The symbol $\mathfrak{W}$ was used since l/h is the wall energy per unit area in units of twice the magnetostatic self-energy per unit surface area of an infinite plate of uniform thickness, h, when it is uniformly magnetized in a direction perpendicular to the surface of the plate.

For the first example, consider the line $\mathfrak{W}\mathfrak{R}'$ for which $l/h = 0.3$, $H/4\pi M_s = 0$. This line has one intersection with F at $\mathfrak{O}(d/h = 0.378)$. Since the slope of F is everywhere positive, there will in general be only one intersection with the construction line for any zero or negative value of $H/4\pi M_s$ independent of the magnitude of l/h. That this single solution is unstable may be appreciated by considering small variations in the solution diameter from its value at $\mathfrak{O}$: Increasing the diameter of the domain from the diameter at $\mathfrak{O}$ increases the magnitude of the internal magnetostatic force term while the other terms remain constant. The total force tending to expand the domain thus increases from zero as the domain expands from the solution diameter. The domain is thus unstable with respect to expansion. An entirely similar argument shows that the domain is unstable with respect to collapse. It is easily seen in general that for a fixed solution diameter the solution will become more unstable (the destabilizing force increasing faster with increasing diameter) as the field is made more negative. Stable solu-

tions to the equilibrium problem exist only for fields aiding the wall field in tending to collapse the domain although one unstable solution exists for any magnitude of negative applied field.

Because of the logarithmic behavior of the force function at large domain diameters, a radially stable solution to the force equation will appear (in addition to the radially unstable solution) when a vanishingly small positive bias field is applied. (Radial stability is determined in the same way as in the preceding paragraph. The existence of radial stability does not assure total domain stability as will be seen.) Since the F function has a negative second derivative everywhere, there can be no solutions in addition to a single radially unstable and a single radially stable solution. This situation is illustrated by the line $\mathfrak{WS}$ in Fig. 2. The line represents $l/h = 0.3$, $H/4\pi M_s = 0.254$ for which the unstable solution, denoted by $\mathfrak{U}$, occurs at $d/h = 0.767$ and the stable solution, denoted by $\mathfrak{S}$, occurs at $d/h = 2.000$. Bobeck[7] has observed experimentally the unstable solution under static conditions which permit the existence of the stable solution. This was done by applying a short duration bias field pulse which reduced the domain diameter from the stable solution diameter at $\mathfrak{S}$ to the unstable solution diameter at $\mathfrak{U}$ and then returning the bias field to its original value just as the unstable solution was attained. The domain having the unstable solution diameter was then stabilized sufficiently by coercivity to allow it to persist.

If the applied field is increased from a value for which there are two solutions, then, the solutions approach each other until at some field value they coalesce. This point at which the solutions coalesce is a point of radial metastability since, at this point, the construction line is tangent to F. Thus, the solution is neither stable nor unstable to lowest order by the small variation argument of the preceding paragraphs. There are no solutions for applied fields greater than the field of radial metastability. Since in this case the inward forces dominate at all diameters, the domain collapses. (Since F everywhere lies below the asymptote d/h, the domains always collapse for applied fields greater than $4\pi M_s$.) In Fig. 2 where $l/h = 0.3$, the collapse point, $\mathfrak{C}$, occurs at $H/4\pi M_s = 0.283$, $d/h = 1.16$. The sequence of the types of solutions which occur as H is varied depends only on the invariant signs of the slope and curvature of F. Therefore for a fixed value of l/h this sequence is independent of the value of l/h. From the slope and curvature properties of F the uniqueness of the collapse diameter and field for a given value of l/h may also be shown. However, the discussion of both this uniqueness and the detailed behavior of the domain diameter

as a function of applied field are conveniently postponed until general stability is discussed.

The device implications of this subsection may be summarized by noting that cylindrical domains exist only in the presence of an applied field applied in a direction tending to collapse the domain and having a magnitude less than $4\pi M_s$.

2.2 *General Stability*

The sign of the second variation of the total domain energy produced by a weak variation in shape characterizes the stability of a cylindrical domain. Since only domains in equilibrium are of interest here, attention is restricted to variations of such domains from their equilibrium size and strictly circular shape. Since an arbitrary weak variation is describable by the expansion (2) with condition (3), the stability problem is reduced to the study of the coefficients of the terms in the energy expansion which are quadratic in the Δr_n and $\Delta\theta_n$. These coefficients are defined (up to some constant factor) as the stiffness matrix elements of the system, and these stiffness matrix elements may clearly be classified as either radial, mixed, or angular stiffness matrix elements.

In the equilibrium energy expansion (7) the only nonzero quadratic coefficients are the coefficients of the $(\Delta r_n)^2$, $n \neq 1$. As required by the cylindrical symmetry of the system, the domain is completely metastable with respect to angle. This is indicated formally in (7) by the absence of any nonzero terms in $\Delta\theta_n\Delta\theta_m$ or $\Delta r_n\Delta\theta_m$. (The angular and mixed stiffness submatrices are identically zero.) Since no terms in $\Delta r_n\Delta r_m$ for $m \neq n$ appear in equation (7), (the radial stiffness matrix is diagonal) the variation amplitudes are quasi-normal-modes of the system. Nonzero terms of order three and higher in the variation amplitudes and angles prevent the variation amplitudes being true normal modes. Finally, since the energy of a domain in an infinite plate is independent of the domain position, the translational stiffness of the domain is zero and therefore since the variation Δr_1 corresponds to lowest order to a translation (see Ref. 1 Sec. 4.2.2), the coefficient of $(\Delta r_1)^2$ in equation (7) is zero.

Since the second-order energy variation with respect to an arbitrary small amplitude weak variation is simply the sum of the energy variations from each normal component of the variation, the study of the stability of circular cylindrical domains reduces to the study of the stability of the domains with respect to size, Δr_0, and shape, Δr_2 to Δr_∞. The sign of the corresponding stiffness matrix element deter-

mines the stability or instability of the domain with respect to the variation of a particular Δr_n. From equation (7), the nonzero normal stiffness matrix elements are

$$\frac{h^2}{4(2\pi M_s^2)(\pi h^3)}\left(\frac{\partial^2 E_T}{\partial r_0^2}\right)_0 = -\left(2\frac{h}{d}\right)\left[\frac{l}{h} - S_0\left(\frac{d}{h}\right)\right] \tag{15a}$$

and

$$\frac{h^2}{4(2\pi M_s^2)(\pi h^3)}\left(\frac{\partial^2 E_T}{\partial r_n^2}\right)_0 = (n^2 - 1)\left(\frac{h}{d}\right)\left[\frac{l}{h} - S_n\left(\frac{d}{h}\right)\right], \qquad n \geqq 2. \tag{15b}$$

The quantities in square brackets are termed stability coefficients. The domain is stable with respect to an arbitrary variation in shape when all of the stiffness matrix elements are positive. From equation (15), this occurs when the $n = 0$ coefficient is negative and all the other stability coefficients are positive,

$$[l/h - S_0(d/h)] < 0 \tag{16a}$$

and

$$[l/h - S_n(d/h)] > 0, \qquad n \geqq 2. \tag{16b}$$

or

$$S_0(d/h) > l/h > S_2(d/h). \tag{17}$$

Since the stability functions have the property,

$$S_{n+1}(d/h) < S_n(d/h), \tag{18}$$

(at least up to $n = 10$ see Ref. 1) the condition for total stability reduces to

$$S_0(d/h) > l/h > S_2(d/h). \tag{19}$$

Since domain stability with respect to Δr_0 and Δr_2 assures total stability, attention is largely restricted to the $n = 0$ and $n = 1$ coefficients. The variations Δr_0 and Δr_2 are termed radial and elliptical variations respectively.

The numerical value of the stability coefficients and in particular the conditions under which the stability coefficients change sign, is determined by a graphical construction, an example of which is now given. The construction of the radial and elliptical stability coefficients for the case $l/h = 0.3$ is shown in Fig. 2. The elevation of the horizontal line $\mathfrak{W}\mathfrak{R}'$ represents the value of l/h. In order to determine the stability coefficients it is necessary to specify an operating diameter which, in

turn, is determined by the applied field. When the domain diameter is greater than the diameter at the intersection of the horizontal line and S_2 at $\mathcal{R}'$ (applied fields less than that represented by the slope of the line $\mathcal{WR}$) the elliptical stability coefficient is negative and the domain is unstable with respect to Δr_2 . The domain diameter at the intersection of the horizontal line and S_2 is called the diameter of elliptical metastability and the corresponding field (the field represented by the slope of the line $\mathcal{WR}$) is termed the field of elliptical metastability. When the diameter is decreased below the diameter of elliptical metastability (by increasing the field above the field of elliptical metastability) the domain becomes stable with respect to elliptical deformation. When the domain diameter is decreased to $d = 2h$ (the corresponding field being represented by the slope of the line $\mathcal{WS}$) the magnitude of the radial stability coefficient (corresponding to the length of $\mathcal{S}'\mathcal{S}_0'$) is approximately equal to the magnitude of the elliptical stability coefficient (corresponding to the length of $\mathcal{S}'\mathcal{S}_2'$).

Increasing the field to the value corresponding to the slope of the line $\mathcal{WC}$, decreases the domain diameter further to the value at the intersection of the horizontal construction line with $\mathcal{S}_0$ at $\mathcal{C}'$, so that the radial stability coefficient is zero and the force equation construction line is tangent to the force curve. Increasing the field above the field value corresponding to the slope of $\mathcal{WC}$ decreases the diameter even further so that the radial stability coefficient becomes positive, the radial stiffness matrix element becomes negative, there are no solutions to the force equation and the domain collapses.

Since the construction line for the force equation is tangent to the force curve at the diameter of radial metastability, it is possible to construct the S_0 curve from the F curve by plotting the loci of points whose ordinate is l/h and whose abscissa is the diameter at which the construction line is tangent to the F curve. Figure 3 illustrates four points of such a construction. Conversely, given the initial slope of F, the S_0 curve may be used to construct F.

In Appendix A of Ref. 1 (see also Fig. 2 here) it was shown that the stability functions are in general monotonic increasing functions of the normalized domain diameter, d/h, and monotonic decreasing functions of the radial periodicity, n (at least up to $n = 10$). From these properties of the S_n functions and the properties of the solution to the force equation discussed in Section 2.1, the following general stability properties may be deduced for any fixed value of l/h: When there is no applied field, the domain diameter is infinite, and the domain is unstable with respect to all variations for which $n \geqq 2$.

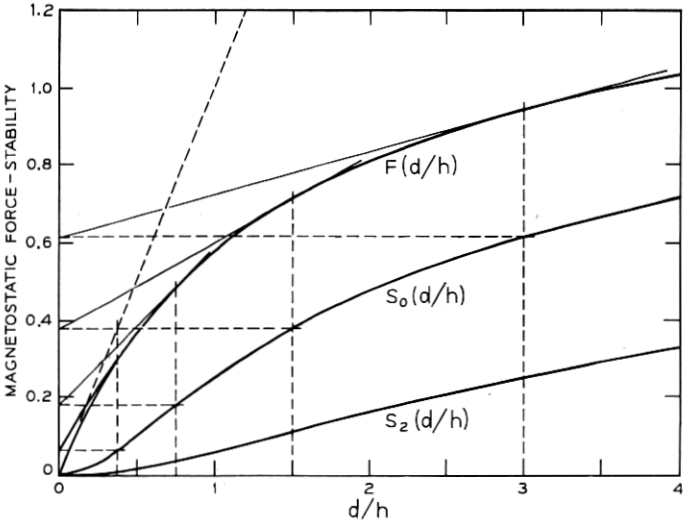

Fig. 3—Construction of the $S_0(d/h)$ function as a sequence of collapse diameter solutions.

When the applied field is small, the diameter is finite and the domain is stable with respect to all variation for which n is equal or greater than some n_m, while remaining unstable with respect to variations of r_n for which $2 \leqq n < n_m$. When the applied field is between the values of elliptical and radial metastability, the domain is stable with respect to all variations. Finally, for applied fields greater than the field of radial metastability, the domain collapses. (As noted previously the domain collapses for applied fields greater than the fields of radial metastability for any value of the domain diameter.)

Note that except for S_1 each S_n forms the boundary between the regions of stability and instability with respect to the corresponding Δr_n and that metastability with respect to each Δr_n $(n \neq 1)$ occurs only along the boundary between the stable and unstable regions.

Even though the radial and elliptical stability functions bound the region of total domain stability, the threefold and fourfold stability functions, S_3 and S_4 , lie quite close to S_2 and it might be expected that when the bias field on a cylindrical domain is reduced in the presence of a small stabilizing coercivity the domain might run out into an initially three or fourfold figure. Such runouts have indeed been observed.[8]

When the bias field on an initially circular stable domain, repre-

sented for example by the line $\mathfrak{WS}$ in Fig. 2, is decreased, $r_b(\theta)$ will increase uniformly for all θ maintaining a circular shape until the point $\mathfrak{R}$ is reached. Increasing the domain radius beyond this value causes the domain to become unstable with respect to elliptical variations. Since for small variations, the variations in the expansion used here are normal modes, the breakaway to instability will not be coupled to any pure radial motion. Thus, when the breakaway occurs $r_b(\theta)$ will actually decrease along one half the length of the wall. Experiments in platelets which have just enough coercivity so that the initiation of the breakaway is observable confirm this somewhat surprising prediction. (See Ref. 4, pp. 1916–1917. The sequence of photographs on these pages were taken with an increasing bias field. The corresponding sequence for a decreasing bias field is similar.)

2.3 *Restrictions Placed on the Possible Region of Device Operation by Stability Considerations*

Since the diameters of radial and elliptical metastability (and the corresponding applied fields) are the boundaries of the region of total stability, they are the boundaries of the region of possible device operation in the hard bubble mode. It is easily appreciated by inspection of equation (15) that the domain will be metastable with respect to a particular Δr_n $(n \neq 1)$ if and only if the corresponding stability coefficient is zero,

$$l/h - S_n(d/h) = 0. \tag{20}$$

Since the S_n are monotonic increasing functions of d/h, a diameter of metastability is uniquely defined for each value of n and characteristic length to thickness ratio,

$$d_n/h = S_n^{-1}(l/h), \qquad n \neq 1. \tag{21}$$

The corresponding applied fields of metastability are then defined using the force equation (14) by

$$\frac{H_n\left(\frac{l}{h}\right)}{4\pi M_s} = \frac{h}{d_n}\left[F\left(\frac{d_n}{h}\right) - \frac{l}{h}\right]. \tag{22}$$

While l/h is a normalized wall energy, it is also, obviously, the reciprocal of the thickness measured in units of the characteristic length. Thus, the d_n and H_n are functions of the normalized thickness, h/l. In the remaining topics of this section it will be appropriate to think of

this parameter as the normalized thickness, since in a given material it is the thickness which is the accessible variable.

In principle, the values of the d_n and H_n for each value of h/l could be obtained by graphical construction. Figure 2 may be taken as an example of such a construction for $h/l = 3.33$ and $n = 0$ and 2. In this construction the intersection at $\mathfrak{C}'$ represents $d_0(0.3) = 1.16$h, the intersection at $\mathfrak{R}'$ represents $d_2(0.3) = 3.58h$, the slope of $\mathfrak{WC}$ represents $H_0(0.3) = 0.283(4\pi M_s)$ and the slope of $\mathfrak{WR}$ represents $H_2(0.3) = 0.196(4\pi M_s)$. (The values quoted here were obtained numerically.)

To better appreciate the way in which the requirements of static stability bound the possible region of device operation, several diameter and applied field functions of the normalized plate thickness have been plotted and their asymptotic forms in the limit of very thick or very thin plates have been computed.

The values used in plotting the functions were obtained in the following way: The implicit equation for d_0 and d_2 [equation (20)] was inverted numerically using the expressions for $S_0(d/h)$ [equation (12)] and S_2(d/h) [equation (13)] to obtain d_0/h and d_2/h as functions of h/l. (Parametric plotting may be used only for functions of a single d_n.) The desired functions were then computed from d_0/h, d_2/h and the expressions for the H_n [equation (22)] and $F(d/h)$ [equation (11)]. (See also Ref. 1, Sections A.1 and A.8.) The asymptotes of the various curves are obtained using the expansions for $F(d/h)$, $S_0(d/h)$ and $S_2(d/h)$ from Appendix B of Ref. 1, with the force equation where necessary (14) and the d_n defining equation (20). The small d/h expansions are carried to order $(d/h)^2$ and the large d/h expansions are carried only to the lowest order constant and log terms in order to facilitate the algebraic inversion of equation (20).

Since the validity of some of the assumptions of the theory increases with increasing d/h, each plot includes an arrow indicating the direction of increasing d_n/h along the plotted curve or curves. The marks at $d_0/h = 1$ and $d_2/h = 1$ indicate the points at which the theory becomes definitely suspect. It has been found experimentally, however, that the theory does give reasonably consistent results for values of d/h which are somewhat less than one.

Figure 4 is a plot of the diameters of radial and elliptical metastability measured in units of the characteristic length, $d_0/l = (h/l)(d_0/h)$ and $d_2/l = (h/l)(d_2/h)$, as functions of the thickness measured in units of the characteristic length, h/l. These diameters have the asymptotic values

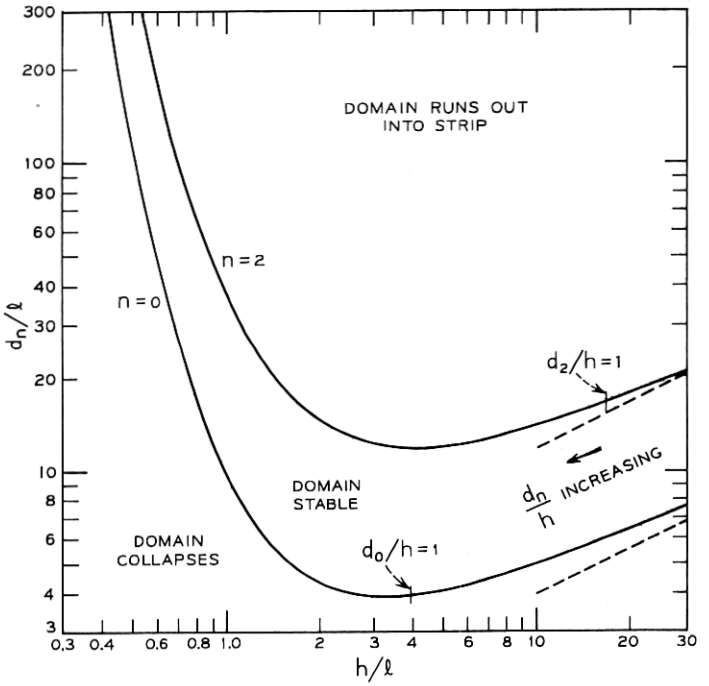

Fig. 4—Diameters of radial and elliptical metastability, d_0 and d_2, in units of the characteristic length, l, as a function of the thickness, h, in units of l.

$$d_0/l \approx 0.412(h/l) \exp(\pi l/h), \qquad h/l \ll 1, \tag{23a}$$

and

$$d_0/l \approx 1.253(h/l)^{\frac{1}{2}}, \qquad h/l \gg 1, \tag{23b}$$

for the collapse diameter, and

$$d_2/l \approx 1.564(h/l) \exp(\pi l/h), \qquad h/l \ll 1, \tag{24a}$$

and

$$d_2/l \approx 3.760(h/l)^{\frac{1}{2}}, \qquad h/l \gg 1, \tag{24b}$$

for the elliptical runout diameter. The uppermost curve in Fig. 5 is a plot of the ratio of the diameter of elliptical metastability to the diameter of radial metastability, $d_2/d_0 = (d_2/h)/(d_0/h) = (d_2/l)/(d_0/l)$, as a function of the h/l. This ratio has the aymptotes

$$d_2/d_0 \approx 3.794, \qquad h/l \ll 1 \tag{25a}$$

and

$$d_2/d_0 \approx 3.000, \qquad h/l \gg 1 \tag{25b}$$

which are easily obtainable from equations (23) and (24). Figure 6 is a plot of the relative variation of the geometric mean of the diameters of radial and elliptical metastability with respect to a relative variation in plate thickness $\partial \ln|(d_0 d_2)^{\frac{1}{2}}|/\partial \ln|h|$ as a function of h/l. This curve has the asymptotes

$$\partial \ln |(d_0 d_2)^{\frac{1}{2}}|/\partial \ln |h| \approx 1.000 - 3.142(h/l)^{-1}, \qquad h/l \gg 1, \tag{26a}$$

and

$$\partial \ln |(d_0 d_2)^{\frac{1}{2}}|/\partial \ln |h| \approx 0.500, \qquad h/l \gg 1. \tag{26b}$$

Inspection of these limiting diameter plots and asymptotic expressions yields the following: In a given material, the minimum stable

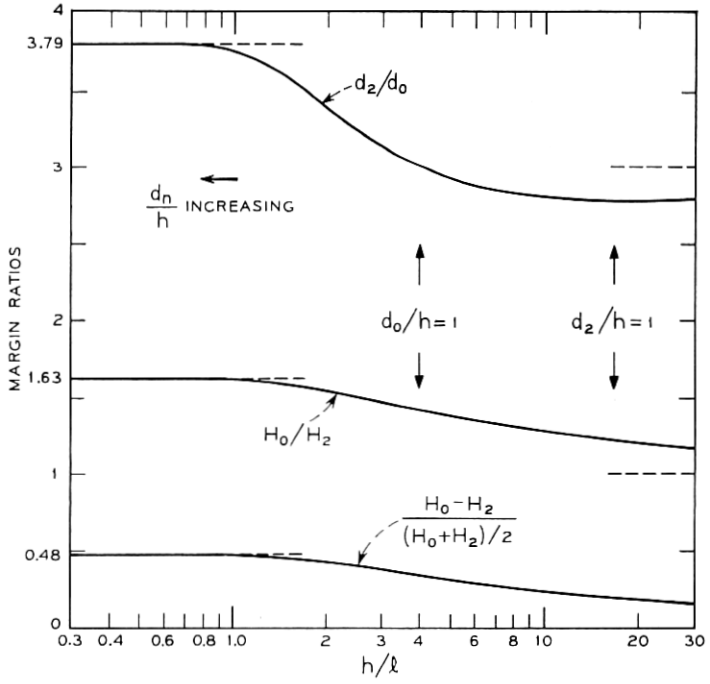

Fig. 5—Diameter and applied field margin ratios, d_2/d_0, H_0/H_2, and $2(H_0 - H_2)/(H_0 + H_2)$, as functions of the thickness, h, measured in units of the characteristic length, l.

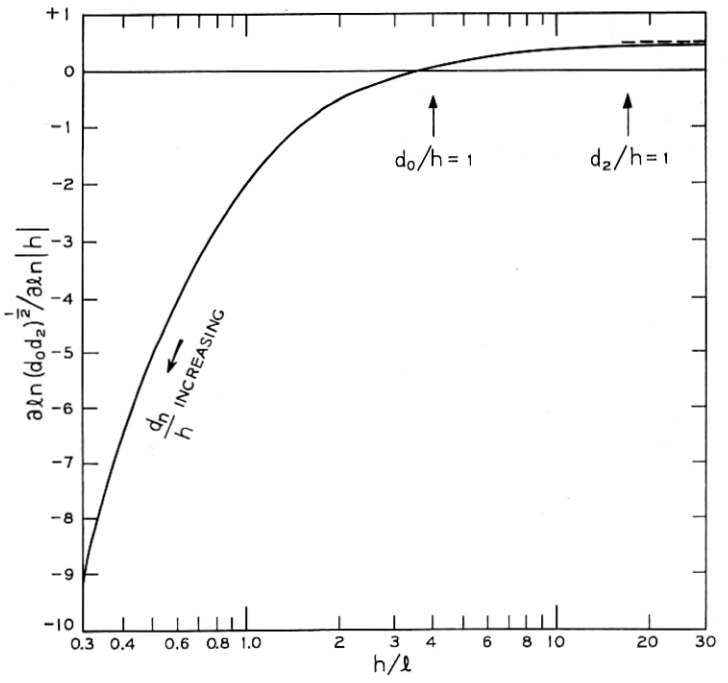

Fig. 6—Logarithmic derivative of the domain diameter with respect to plate thickness, $\partial \ln d/\partial \ln |h|$, for the bias condition $d = (d_0 d_2)^{\frac{1}{2}}$ as a function of the plate thickness, h, measured in units of the characteristic length, l.

diameter attainable for any plate thickness is $\approx 3.9l$ at a thickness of $\approx 3.3l$. The minimum diameter of elliptical instability is $\approx 12l$ attained at a thickness of $\approx 4.2l$. For any given plate thickness, the range of diameters over which the domain is stable is small, the ratio of the diameter of elliptical metastability to the diameter of radial metastability being roughly equal to three for any plate thickness. The domain diameter is thus for all practical purposes determined once the plate thickness and characteristic length are known. The increase in domain diameter with increasing plate thickness in thick plates is quite mild being according to a square root law. The increase in domain diameter with decreasing plate thickness is, on the other hand, exponential for a thin plate. This variation is so rapid that the magnitude of the relative variation of the diameter of a centrally biased domain, $d = (d_0 d_2)^{\frac{1}{2}}$ with respect to a relative variation in thickness increases according to the inverse of the thickness.

Figure 7 is a plot of the applied fields of radial and elliptical metastability, $H_0/4\pi M_s = (h/d_0)[F(d_0/h) - l/h]$ and $H_2/4\pi M_s = (h/d_2)[F(d_2/h) - l/h]$, as functions of h/l. These curves have the asymptotes

$$H_0/4\pi M_s \approx 0.772 \exp(-\pi l/h), \qquad h/l \ll 1, \tag{27a}$$

and

$$H_0/4\pi M_s \approx 1.000 - 1.596(h/l)^{-\frac{1}{2}}, \qquad h/l \gg 1, \tag{27b}$$

for the collapse field and

$$H_2/4\pi M_s \approx 0.475 \exp(-\pi l/h), \qquad h/l \ll 1, \tag{28a}$$

and

$$H_2/4\pi M_s \approx 1.000 - 2.660(h/l)^{-\frac{1}{2}}, \qquad h/l \gg 1, \tag{28b}$$

for the elliptical runout field. The two lowermost curves in Fig. 5 are

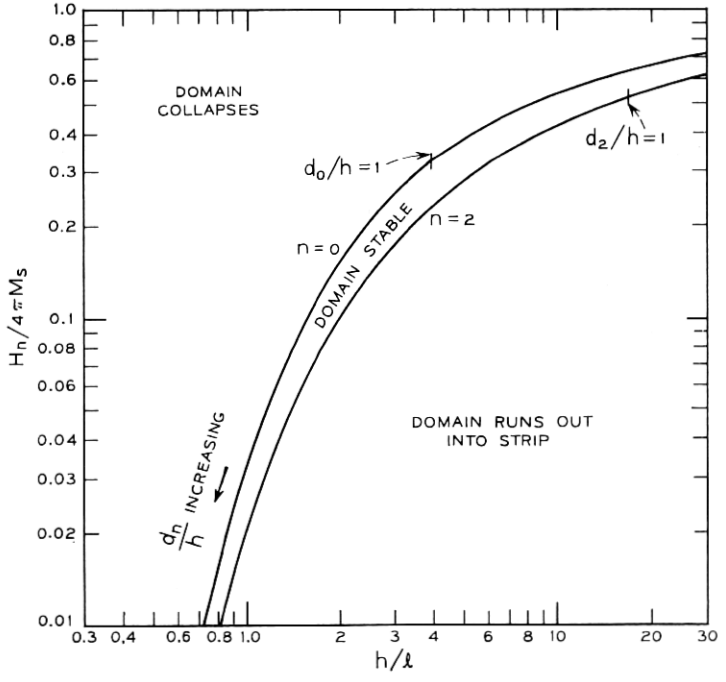

Fig. 7—Applied fields of radial and elliptical metastability, H_0 and H_2, in units of $4\pi M_s$ as a function of thickness, h, measured in units of the characteristic length, l.

plots of the ratio of the collapse field to the elliptical runout field and the ratio of the difference of these fields to their average as functions of h/l. The asymptotes of these ratios are

$$H_0/H_2 \approx 1.626, \qquad h/l \ll 1, \tag{29a}$$

and

$$H_0/H_2 \approx 1.000 + 1.064(h/l)^{-\frac{1}{2}}, \qquad h/l \gg 1, \tag{29b}$$

for the field ratio and

$$2(H_0 - H_2)/(H_0 + H_2) \approx 0.477, \qquad h/l \ll 1, \tag{30a}$$

and

$$2(H_0 - H_2)/(H_0 + H_2) \approx 1.064(h/l)^{-\frac{1}{2}}, \qquad h/l \gg 1, \tag{30b}$$

for the ratio of the difference of the fields to their average. Equations (29) and (30) are easily obtainable from equations (27) and (28).

Inspection of these limiting applied field plots and asymptotes yields the following: The field magnitudes decrease exponentially with decreasing plate thickness, rapidly becoming unmanageably small for very thin plates. The fields increase monotonically with increasing plate thickness toward the common value, $4\pi M_s$. The relative variation of applied fields, allowed within the region of stable circular domains, is smaller than the allowed relative variation of diameters, approaching a constant for thin plates and zero for thick plates.

Note that $4\pi M_s$ determinations are most accurately carried out in moderately thick plates (within the limits of the cylindrical wall approximation and the coercivity limits described in the next section) since here $H_0/4\pi M_s$ (and $H_2/4\pi M_s$) is a weak function of l and is asymptotic to one. Measurements of the characteristic length, on the other hand, are best carried out in moderately thin plates (within coercivity limits) where the diameter is a strong function of l. The appreciation of the validity of these statements will be greatly enhanced if the reader will try a few constructions on a plot of the F and S_n functions.

The implications of the foregoing for device design are summarized as follows: For a given value of h/l there is only an approximately three-to-one variation in the domain diameter permitted within the stable region so that given material and plate thickness, domain size is closely determined. The minimum domain diameter occurs for $h/l \approx 4$. For thinner and thinner plates, both the plate thickness

margins and the applied field magnitude decrease exponentially. While field margins are reasonable for $h/l \approx 4$ $(H_0/H_2 = 1.41)$ [or $2(H_0 - H_2)/(H_0 + H_2) \approx 0.34$], they become vanishingly small in very thick plates. These considerations thus demonstrate that from stability considerations alone, for a given value of the characteristic length, there is both a preferred range of thicknesses and a preferred range of domain diameters (or applied fields) for device operation. The preferred range of each is centered about the preferred values

$$h_p = 4l \tag{31}$$

and

$$d_p = 8l \tag{32}$$

for which the bias field is

$$H_p = 0.279(4\pi M_s). \tag{33}$$

These values will be shown to be preferred in another sense in the next section.

2.4 *Domain Diameter as a Function of Applied Field*

Since domain diameter is in practice only measurable for diameters between d_0 and d_2 (applied fields between H_0 and H_2), these points form natural endpoints for plotting the diameter as a function of applied field. Figure 8 is a plot of $(d - d_0)/(d_2 - d_0)$, as a function of $(H - H_2)/(H_0 - H_2)$, for various values of the normal thickness in the infinite disk. The plots for finite nonzero values of the thickness were obtained numerically using the force equation (14), the defining relation for the d_n [equation (21)] and the expressions for F [equation (11)], S_0 [equation (12)] and S_2 [equation (13)]. In the limit of very thick plates, diameter and applied field are related by

$$\frac{H_0 - H}{H_0 - H_2} = \frac{3}{4}\frac{(d - d_0)^2}{dd_0}, \qquad h \to \infty \tag{34a}$$

using the small d/h expansions of F, S_0 and S_2 from Ref. 1, Appendix B, to order $(d/h)^2$. In the limit of very thin plates, diameter and applied field are related by

$$\frac{H_0 - H}{H_0 - H_2} = \frac{1}{1 - \frac{7}{3}\exp(-\frac{4}{3})}\left[1 - \frac{d_0}{d}\left(1 + \ln\left|\frac{d}{d_0}\right|\right)\right], \qquad h \to 0 \tag{34b}$$

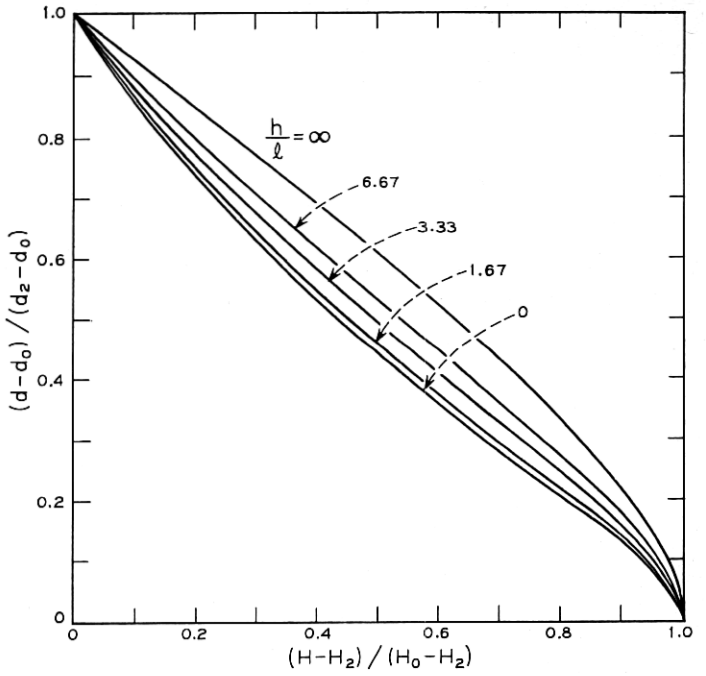

Fig. 8—Relative diameter, $(d - d_0)/(d_2 - d_0)$, as a function of relative applied field, $(H - H_2)/(H_0 - H_2)$, in the infinite plate for various values of the plate thickness, h, measured in units of the characteristic length, l.

using the constant and simple log terms of the expansions of F, S_0 and S_2 from Appendix B of Ref. 1. The curves for intermediate thicknesses are seen to lie, in order, between the limiting curves and are all nearly linear except in the neighborhood of the collapse diameter. In the neighborhood of the collapse diameter, the slopes of all the curves are infinite. This is easily appreciated by expressing the derivative of the domain diameter with respect to applied field in terms of the radial stability coefficient.

The derivative of the domain diameter with respect to the applied field is obtained by considering equation (14) to be continuously solved and then differentiating with respect to d to obtain

$$\frac{1}{4\pi M_s}\left(\frac{d}{h}\frac{\partial H}{\partial d} + \frac{1}{h}H\right) - \frac{\partial}{\partial d}F(d/h) = 0. \tag{35}$$

Eliminating H with the force equation, using the equation for S_0 (12)

and rearranging yields

$$\frac{4\pi M_s}{d}\frac{\partial d}{\partial H} = \frac{d}{h}\frac{1}{l/h - S_0\left(\frac{d}{h}\right)}. \tag{36}$$

So that indeed the derivative of diameter with respect to applied field approaches infinity as radial metastability is approached.

2.5 *The Effect of Wall Energy Anisotropy on the Size, Shape and Stability of Cylindrical Domains*

The domains observed in orthoferrites are never precisely circular but always have some degree of ellipticity. The present subsection relates this anisotropy in domain shape to more fundamental domain parameters.

In the orthoferrites $K_u \gg 2\pi M_s^2$ so that the magnetization lies rigidly along the plate normal and the wall width is narrow as compared to the domain diameter (1). The applied field energy, E_H and the internal magnetostatic energy, E_M , terms of the total energy expression (4) thus make no contribution to producing the domain anisotropy. Therefore the anisotropy results from an anisotropy in the wall energy density σ_w . Considering again the wall energy density to be independent of wall curvature and the wall to be oriented with its normal perpendicular to the plate normal, i.e., a cylindrical wall, the wall energy density may be expanded as

$$\sigma_w = \bar{\sigma}_w + \tfrac{1}{2}\sum_{n=1}^{\infty}\sigma_{2n}\cos\left[2n(\nu - \nu_{2n})\right] \tag{37}$$

where ν is the angle between the wall normal, **N**, and the x axis (see Fig. 9) and the expansion coefficients, $\bar{\sigma}_w$, σ_{2n} and ν_{2n} are taken to be positive. The odd angular periodicity expansion coefficients are deleted from equation (37) since the energy of the system is invariant under time reversal while the direction of the wall normal (referred to the magnetization direction) changes sign.

To describe the anisotropy observed in orthoferrites, it has proven sufficient to include only the average and two-fold terms in equation (37). In addition, if the plate is assumed oriented so that the wall energy is maximized when the wall normal lies along the x axis, the wall energy density is

$$\sigma_w = \bar{\sigma}_w + \tfrac{1}{2}\Delta\sigma_w \cos 2\nu. \tag{38}$$

Although the method which now will be employed to calculate the

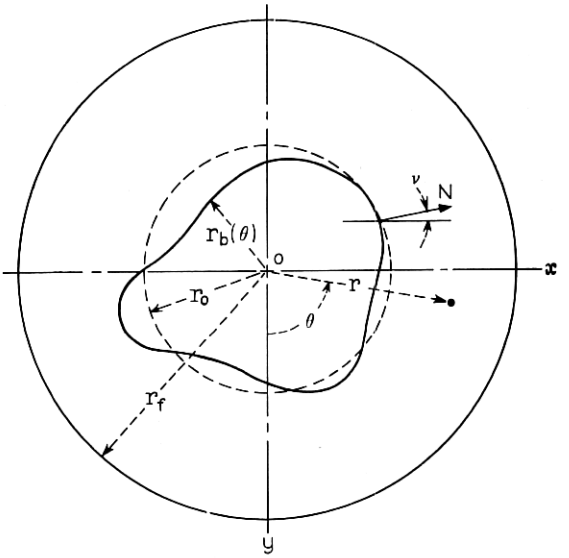

Fig. 9—Coordinate system used in consideration of anisotropic wall energy.

implications of equation (38) is clearly applicable to the more general energy expression (37), attention will be restricted to equation (38).

The total wall energy is

$$E_W = h \oint \sigma_w \, ds \tag{39}$$

where s is the arc length along the curve describing the domain shape in the plane. When the wall energy density (38) is substituted into equation (39) and the differential arc length, ds, and the wall normal orientation angle, ν (see Fig. 9), are expressed in terms of θ, $r_b(\theta)$ and $\partial r_b(\theta)/\partial\theta$, the total wall energy expression becomes

$$\begin{aligned} E_W = {} & h\bar{\sigma}_w \int_0^{2\pi} \left[r_b^2 + \left(\frac{\partial r_b}{\partial \theta} \right)^2 \right]^{\frac{1}{2}} d\theta \\ & + \tfrac{1}{2} h \, \Delta\sigma_w \int_0^{2\pi} \left\{ \left[r_b^2 + \left(\frac{\partial r_b}{\partial \theta} \right)^2 \right]^{\frac{1}{2}} \cos 2\theta \right. \\ & \left. - 2 \frac{\partial r_b}{\partial \theta} \left(\frac{\partial r_b}{\partial \theta} \cos 2\theta - r_b \sin 2\theta \right) \left[r_b^2 + \left(\frac{\partial r_b}{\partial \theta} \right)^2 \right]^{-\frac{1}{2}} \right\} d\theta. \end{aligned} \tag{40}$$

In the isotropic wall energy density case, $\sigma_w = \bar{\sigma}_w$, the first term in equation (40) is identical to the isotropic wall energy expression [equation (8) of Ref. 1], the second term in equation (40) representing entirely the effect of the wall energy anisotropy.

To evaluate the effect of the anisotropy term even to lowest order, it is necessary to obtain all the first and second derivatives with respect to the expansion coefficients, Δr_n and $\Delta\theta_n$ of the expansion of $r_b(\theta)$ (2) for the case of a strictly circular domain $r_b(\theta) = r_0$. In the expressions for the derivatives, $\partial\Delta r_n$ and $\partial\Delta\theta_n$ are again abbreviated to ∂r_n and $\partial\theta_n$ and evaluation at $r_b(\theta) = r_0$ is denoted by a zero subscript. The first derivative with respect to Δr_n is

$$\frac{\partial E_W}{\partial r_n} = h\bar{\sigma}_w \int_0^{2\pi} \left\{ r_b \frac{\partial r_b}{\partial r_n} + \frac{\partial r_b}{\partial \theta} \frac{\partial\left(\frac{\partial r_b}{\partial \theta}\right)}{\partial r_n} \right\} \left[r_b^2 + \left(\frac{\partial r_b}{\partial \theta}\right)^2 \right]^{-\frac{1}{2}} d\theta$$

$$+ \tfrac{1}{2} h\, \Delta\sigma_w \int_0^{2\pi} \left\{ \left[r_b \frac{\partial r_b}{\partial r_n} + \frac{\partial r_b}{\partial \theta} \frac{\partial\left(\frac{\partial r_b}{\partial \theta}\right)}{\partial r_n} \right] \left[r_b^2 + \left(\frac{\partial r_b}{\partial \theta}\right)^2 \right]^{-\frac{1}{2}} \cos 2\theta \right.$$

$$- 2 \frac{\partial\left(\frac{\partial r_b}{\partial \theta}\right)}{\partial r_n} \left(\frac{\partial r_b}{\partial \theta} \cos 2\theta - r_b \sin 2\theta \right) \left[r_b^2 + \left(\frac{\partial r_b}{\partial \theta}\right)^2 \right]^{-\frac{1}{2}}$$

$$\left. - 2 \frac{\partial r_b}{\partial \theta} \frac{\partial}{\partial r_n} \left[\left(\frac{\partial r_b}{\partial \theta} \cos 2\theta - r_b \sin 2\theta \right) \left(r_b^2 + \left(\frac{\partial r_b}{\partial \theta}\right)^2 \right)^{-\frac{1}{2}} \right] \right\} d\theta. \quad (41)$$

Setting $r_b = r_0$ and $\partial r_b/\partial\theta = 0$ and carrying out the integration yields

$$\left(\frac{\partial E_W}{\partial r_n}\right)_0 = 2\pi h\bar{\sigma}_w\, \delta_{n0} - \frac{3\pi}{2} h\, \Delta\sigma_w\, \delta_{n2} \cos 2\theta_2 \quad (42a)$$

where δ_{mn} is the Kronecker delta function. The remaining derivatives which are evaluated in an entirely similar manner are:

$$\left(\frac{\partial E_W}{\partial \theta_n}\right)_0 = 0, \quad (42b)$$

$$\left(\frac{\partial^2 E_W}{\partial r_m\, \partial r_n}\right)_0 = \frac{\pi}{r_0} h\bar{\sigma}_w n^2\, \delta_{mn}$$

$$+ \frac{3\pi}{4r_0} h\, \Delta\sigma_w mn \{ \delta_{n1}\, \delta_{m1} \cos 2\theta_1 - \delta_{n,m\pm 2} \cos (n\theta_n - m\theta_m) \}, \quad (42c)$$

$$\left(\frac{\partial^2 E_W}{\partial\theta_m\,\partial\theta_n}\right)_0 = 0, \tag{42d}$$

and

$$\left(\frac{\partial^2 E_W}{\partial\theta_m\,\partial r_n}\right)_0 = 3\pi h\,\Delta\sigma_w\,\delta_{m2}\,\delta_{n2}\sin 2\theta_2\ . \tag{42e}$$

The terms of equation (42) in $\bar{\sigma}_w$ are all identical to the corresponding terms in the isotropic case [equation (14) of Ref. 1] so that adding the terms of equation (42) in $\Delta\sigma_w$ to equation (7) yields the total energy expansion for the anisotropic case. The domain is therefore in equilibrium when the force equation for the isotropic case (14) with $\sigma_w = \bar{\sigma}_w$ is solved and the force tending to make the domain elliptical is somehow balanced. Inclusion of the effect of second order energy variations terms solves the latter part of the equilibrium problem to lowest order.

Before proceeding with this solution, it is appropriate to comment upon the significance of the various energy terms. As required by translational symmetry [Ref. 1, Sec. 4.2.2] $(\partial E_{\Delta W}/\partial r_2)_0 = -2r_0\cdot(\partial^2 E_{\Delta W}/\partial r_1^2)_0$ when $\theta_1 = \theta_2$ where $E_{\Delta W}$ is the $\Delta\sigma_W$ contribution to the energy. The $(\partial^2 E_W/\partial r_1^2)_0$ term in the stiffness matrix thus has only kinematic significance. On the other hand, $-\partial[\Delta r_2(\partial E_W/\partial r_2)_0]/\partial\theta_2 = -\Delta r_2(\partial E_W/\partial\theta_2\,\partial r_2)_0$ is a torque tending to turn an elliptical domain into the direction in which the force tending to make the domain elliptical is most positive.

To solve the elliptical equilibrium problem, it is convenient to write the energy variation expression in the form

$$\Delta E_T = -\mathbf{F}\cdot\mathbf{X} + \tfrac{1}{2}\mathbf{X}\cdot\mathbf{S}\cdot\mathbf{X} + 0_3(\mathbf{X}) \tag{43a}$$

where

$$\mathbf{X} \equiv [x_1\ ,\ x_2\ ,\ x_3\ ,\ x_4\ ,\ x_5\ ,\ x_6\ ,\ x_7\ ,\ \cdots] \tag{43b}$$

$$\equiv [\Delta r_0\ ,\ \Delta r_1\ ,\ \Delta\theta_1\ ,\ \Delta r_2\ ,\ \Delta\theta_2\ ,\ \Delta r_3\ ,\ \Delta\theta_3\ ,\ \cdots] \tag{43c}$$

and where the elements of the force vector, F, and the stiffness matrix, S, are

$$F_i = -\left(\frac{\partial E_T}{\partial x_i}\right)_0 \tag{43d}$$

and

$$S_{ij} = \left(\frac{\partial E_T}{\partial x_i\,\partial x_j}\right)_0\ . \tag{43e}$$

Setting the gradient of the total energy in the space of the x_i equal to zero and solving for the equilibrium yields displacements when third order energy terms are neglected

$$\mathbf{X} = \mathbf{S}^{-1}\mathbf{F} \tag{44}$$

where $\mathbf{S}^{-1}$ is the inverse stiffness or compliance matrix. From the comments in the preceding two paragraphs and inspection of equations (43) and (44), it can be seen that stable equilibrium is obtained when: r_0 is the stable solution to the isotropic force equation (14) with $\sigma_w = \bar{\sigma}_w$, $\theta_n = 0$ and $\Delta\theta_n = 0$ for all n (allowing now negative values of Δr_n) and $\Delta r_n = 0$ for $n = 0$ and n odd. The remaining even n Δr_n are determined from equation (44) written with respect to these variables only. Because of the special form of the resulting F and S, inverting only a finite submatrix of S yields X to any finite order in $\Delta\sigma_w$. When this is done there results

$$\frac{\Delta r_2}{r_0} = \frac{1}{2}\left[\frac{l}{h} - S_2\left(\frac{d}{h}\right)\right]^{-1}\left(\frac{\Delta l}{h}\right) + O_3\left(\frac{\Delta l}{h}\right), \tag{45a}$$

$$\frac{\Delta r_4}{r_0} = \frac{1}{5}\left[\frac{l}{h} - S_2\left(\frac{d}{h}\right)\right]^{-1}\left[\frac{l}{h} - S_4\left(\frac{d}{h}\right)\right]^{-1}\left(\frac{\Delta l}{h}\right)^2 + O_4\left(\frac{\Delta l}{h}\right), \tag{45b}$$

$$\frac{\Delta r_n}{r_0} = O_3\left(\frac{\Delta l}{h}\right), \qquad n \geqq 6, \tag{45c}$$

where

$$\Delta l \equiv \Delta\sigma_w/4\pi M_s^2 . \tag{46}$$

Equation (45a) has also been obtained by E. Della Torre and M. Dimyan.[9]

In the small Δr_n approximation of this calculation the wall anisotropy term has no effect on r_0 or any of the odd n Δr_n. The collapse diameter, d_0, and collapse field, H_0, are thus unchanged with respect to the isotropic case. At all diameters, however, the anisotropy pulls the initially circular domain out into an elliptical shape, the ellipticity being smallest at the collapse diameter and blowing up to infinity at the isotropic elliptical runout diameter (45a). At the isotropic runout diameter this calculation clearly cannot be applied to obtaining the reduction in the range of stability which wall anisotropy produces. It is also clear from the blow up of Δr_2 that any statement of such a reduction in the region of stability should be in terms of applied fields rather than domain diameters. In calculations of $\bar{\sigma}_w$ and $\Delta\sigma_w$ from measurements of the major and minor axes of elliptical domains, it should be noted

that $\Delta r_4/r_0$ [equation (45b)] makes a small contribution to the length of each axis which is not removed by averaging.

In platelets having the preferred thickness, $h = 4l$, and biased to the collapse diameter, $\Delta r_2/r_0 = 2.61(\Delta l/h)$ and $\Delta r_4/r_0 = 4.65(\Delta l/h)^2$, while in the neighborhood of the isotropic elliptical runout diameter where $\Delta r_2 \to \infty$, $\Delta r_4/r_0 = 3.59(\Delta l/h)\ \Delta r_2/r_0$.

In rare earth orthoferrites, the anisotropy in wall energy is typically (within a factor of two) $\Delta\sigma_w/\bar{\sigma}_w = 3\%$ so that $\Delta l/h$ for $h = 4l$ is only $3/4\%$. The ellipticity at collapse is thus small. The contribution of Δr_4 is very small at all diameters ($h = 4l$) and further, near collapse, the cylindrical wall and infinitesimal wall width approximations quite possibly produce larger errors.

The implication of the foregoing for device applications is that wall energy anisotropy has no effect upon the collapse diameter and collapse field. As far as the elliptical runout conditions are concerned, careful measurements carried out on a low coercivity platelet of $TmFeO_3$ in which $\Delta\sigma_w/\bar{\sigma}_w = 3\%$ show that the reduction in the ratio of the collapse to the elliptical runout field is only of the order of 1%.[10]

III. COERCIVITY AND MOBILITY

The preceding sections treated only forces arising from reversible processes. The present section considers forces arising from the irreversible processes describable by the wall motion coercivity and wall mobility. Several relations between wall parameters and domain parameters are obtained. In particular, this section computes the domain coercivity and mobility in terms of the wall coercivity and obtains the maximum allowable coercivity which permits device operation in the hard bubble mode. Inversely, it is shown how the wall mobility and coercivity may be obtained by domain measurements.

3.1 *Domain Dissipation*

The method used to take dissipative effects into account is to compute the power dissipation produced by a general variation in domain shape using the wall dissipation equation and then to set this equal to the power produced by the variation. By this procedure the equations for the various modes (translation, size change and deformation) are obtained. The dissipation equation approach is taken as a best first guess to the solution of coercivity problems. The reader is cautioned not to take any of the coercivity results too literally, since

coercivity is never uniform and in many cases depends on the direction of wall motion.[11]

Wall motion in many materials is describable in terms of a wall motion coercivity and a wall motion mobility.[12–14] Such a description should be valid in any material for sufficiently low velocities and coercivities. Presently known uniaxial materials such as $BaFe_{12}O_{19}$ for which the velocity-drive field relation is not describable by coercivity and mobility at high drive fields[15–18] (they show roughly a limiting velocity) have low mobilities which reduce their usefulness in device applications. The present work therefore restricts attention to 180° domain walls in materials having the velocity-drive field relation

$$|v_n| = \begin{cases} \mu_w(|H_L| - H_c), & |H_L| > H_c \,, \\ 0, & |H_L| \leqq H_c \,, \end{cases} \tag{47}$$

where: v_n is the local wall velocity in a direction normal to the wall, H_L is the total local field component parallel to the magnetization, and where equation (47) serves as the defining relation for the wall motion coercive field, H_c, and the wall mobility μ_w. The field H_L includes the effect of all magnetic fields as well as any effective fields such as the "wall energy field," and may vary from point to point. The symbol, H_L, is used to distinguish it from H, used elsewhere to denote the spatially uniform z component of the applied field. For a planar wall in the absence of internal magnetostatic forces, H_L is the applied field. Equation (47) is assumed to hold whether or not the wall is accelerating since for presently known materials wall inertia effects are negligible.

Consider now a segment of 180° domain wall such as a portion of the domain wall shown in Fig. 1 and assume that H_L is positive when it lies in the positive z direction. Under these conditions, the power input per unit area from the local field to an inward moving (decreasing r_b) segment of the domain wall is independent of the details of the magnetic configuration within the wall and is

$$\rho_{in} = 2M_s\,|H_L v_n|. \tag{48}$$

Since inertial effects have been assumed to be negligible, the power input must be equal to the power dissipated per unit wall area, ρ_{diss}, so that eliminating H_L from equations (47) and (48) results in

$$\rho_{diss} = 2M_s\left[H_c\,|v_n| + \frac{1}{\mu_w}v_n^2\right]. \tag{49}$$

Integrating the dissipation density over the domain wall area yields the total dissipation

$$P_{\text{diss}} = \int_{\text{wall}} 2M_s\left[H_c\,|v_n| + \frac{1}{\mu_w}v_n^2\right]d\alpha \tag{50}$$

where $d\alpha$ is the differential wall area. For a circular domain, where $r_b(\theta) = r_0$, this expression becomes

$$P_{\text{diss}} = 2M_s h r_0 \int_0^{2\pi}\left[H_c\,|\mathbf{v}\cdot\mathbf{i}_r| + \frac{1}{\mu_w}|\mathbf{v}\cdot\mathbf{i}_r|^2\right]d\theta \tag{51}$$

where $\mathbf{i}_r$ is the unit vector in the radial direction. Now for a circular domain

$$\begin{aligned}\mathbf{v}\cdot\mathbf{i}_r &= \frac{dr_b(\theta)}{dt}\\ &= \sum_{n=0}^{\infty}\left[\left(\frac{\partial r_b(\theta)}{\partial r_n}\right)_0\frac{dr_n}{dt} + \left(\frac{\partial r_b}{\partial\theta_n}\right)\frac{d\theta_n}{dt}\right]\\ &= \sum_{n=0}^{\infty}\cos\left[n(\theta-\theta_n)\right]\frac{dr_n}{dt}\end{aligned} \tag{52}$$

where again $d\Delta r_n$ and $d\Delta\theta_n$ have been abbreviated to dr_n and $d\theta_n$. Substituting equation (52) into equation (51) and carrying out the integration yields

$$\begin{aligned}P_{\text{diss}} = 4\pi M_s h r_0\Bigg\{H_c\Bigg[\left|\frac{dr_0}{dt}\right| + \frac{2}{\pi}\sum_{n=1}^{\infty}\left|\frac{dr_n}{dt}\right| + NO_1\left(\frac{dr_n}{dt}\right)\Bigg]\\ + \frac{1}{\mu_w}\left[\left(\frac{dr_0}{dt}\right)^2 + \frac{1}{2}\sum_{n=1}^{\infty}\left(\frac{dr_n}{dt}\right)^2 + O_3\left(\frac{dr_n}{dt}\right)\right]\Bigg\}\end{aligned} \tag{53}$$

where $NO_1\ (dr_n/dt)$ indicates the nonlinear coercivity coupling terms which appear even in lowest order. The nonlinear coupling terms tend in general to couple in additional modes even when only one dr_n/dt is initially nonzero. An exception to this is the uniform radial mode of motion dr_0/dt which, because of its symmetry, may take place without coupling in the other modes. If the coercivity is negligible $[H_c \ll 1/\mu_w(dr_n/dt)]$ then the Δr_n and $\Delta\theta_n$ remain uncoupled normal modes of the system. The consequences of the damping of the various individual modes will now be considered in the order $n = 1$, $n = 0$, $n \geqq 2$.

3.2 *Domain Coercivity and Mobility* ($n = 1$)

Consider an initially circular domain in which only $d\Delta r_1/dt$ is nonzero. In this case the component of the domain wall velocity

normal to the wall is

$$v_n = dr_b(\theta)/dt = (d\Delta r_1/dt) \cos(\theta - \theta_1). \tag{54}$$

Since the distribution of the wall velocity component normal to the domain wall for a circular domain propagating with velocity, v_d, in the θ_d direction is

$$v_n = \mathbf{i}_r \cdot \mathbf{v}_d = |v_d| \cos(\theta - \theta_d), \tag{55}$$

a variation in Δr_1 may be identified with translation in the θ_d direction with

$$|\mathbf{v}_d| = |d\Delta r_1/dt|. \tag{56}$$

Using equation (53), the power dissipated by a uniformly moving circular domain is

$$P_{\text{diss}} = \pi M_s h r_0 \left[\frac{8}{\pi} H_c |\mathbf{v}_d| + \frac{2}{\mu_w} \mathbf{v}_d^2\right] \tag{57}$$

and, since $P_{\text{diss}} = -\mathbf{v}_d \cdot \mathbf{F}_d$ where $\mathbf{F}_d$ is the drag force, the equivalent force for a domain moving with a nonzero velocity is

$$\mathbf{F}_d = -\pi M_s h r_0 \left[\frac{8}{\pi} H_c + \frac{2}{\mu_w} |\mathbf{v}_d|\right] \mathbf{i}_v \tag{58}$$

where $\mathbf{i}_v = \mathbf{v}_d/|\mathbf{v}_d|$ is the unit vector in the direction of the motion. Notice that $\mathbf{F}_d$ is an ordinary linear force which could be measured mechanically with the aid of a magnetic probe.

Translational forces are most easily produced by gradients in the applied field. The power input to the domain from such a force is obtained by integrating the power input density, equation (48), over the domain wall area. In the case of a uniform gradient the local field at the domain wall is

$$H_L = \bar{H}_L - \tfrac{1}{2} |\Delta \mathbf{H}| \cos(\theta - \theta_g) \tag{59}$$

where $\Delta \mathbf{H}$ is a vector orientated in the direction in which the bias field decreases most rapidly, θ_g, and has a magnitude equal to the maximum difference in field across the domain (a gradient of magnitude $|\Delta H|/2r_0$ and direction $\theta_g + \pi$). In equation (59) $\bar{H}_L$ includes: the bias field at the center of the domain, the "wall field" and the demagnetizing field, all of which are independent of angle. All of the field components in equation (59), H_L, $\bar{H}_L$ and $\Delta \mathbf{H}$ are to be understood as the z-averaged z components of the actual field since this is the quantity which interacts with a 180° cylindrical domain wall. With this understanding, integration over the wall area may be replaced by

multiplication by h and integration over θ. Assuming the domain to be exactly circular, the total power input to the domain is

$$P_{in} = 2M_s r_0 h \cdot \int_0^{2\pi} [\bar{H}_L - \tfrac{1}{2}|\Delta\mathbf{H}| \cos(\theta - \theta_v)] \cdot [-|v_d| \cos(\theta - \theta_d)]\, d\theta$$

$$= \pi r_0 h M_s \, \Delta\mathbf{H} \cdot \mathbf{v}_d \tag{60}$$

which is just the expression for the power input to a dipole of strength $(\pi r_0^2 h)(2M_s)$ propagating in a gradient of magnitude $|\Delta\mathbf{H}|/2r_0$.

The domain will propagate in the direction in which the input power is greatest, ($\theta_v = \theta_d$ the direction in which the bias field decreases most rapidly), and the magnitude of the velocity will be such that the dissipated power (57) balances the input power (60). Such a balance always occurs for $v_d = 0$. When $|\Delta\mathbf{H}| \leqq (8/\pi)H_c$ this is the only condition in which the balance is maintained. The domain velocity is therefore

$$|\mathbf{v}_d| = \frac{1}{2}\mu_w\left(|\Delta H| - \frac{8}{\pi}\mathbf{H}_c\right), \qquad |\Delta\mathbf{H}| > \frac{8}{\pi}H_c, \tag{61a}$$

$$|\mathbf{v}_d| = 0, \qquad |\Delta\mathbf{H}| \leqq \frac{8}{\pi}H_c. \tag{61b}$$

Comparison of equations (47) and (61) shows that it is possible to define a domain mobility and coercivity by taking $\Delta\mathbf{H}$ as the driving field in terms of the wall mobility and coercivity as

$$\mu_d = \tfrac{1}{2}\mu_w \tag{62}$$

and

$$H_{cd} = \frac{8}{\pi}H_c \tag{63}$$

if $\Delta\mathbf{H}$ is taken to be the drive field.

Note that in the integral for the power input (60), the angle independent field term, $\bar{H}_L$, does not contribute so that the effective power input density with respect to angle for a domain propagating down a bias field gradient is $r_0 h M_s |\Delta\mathbf{H}| |\mathbf{v}_d| \cos^2(\theta - \theta_d)$ which has the same angular factor as the mobility associated dissipation (50) and (55). The power input and power dissipated thus cancel (after z averaging) at each point on the perimeter of the domain for domains propagating under the influence of a uniform field gradient and viscous damping. In this case therefore there are no forces tending to distort the domain shape from circular. When coercivity is present (even perfectly uniform

coercivity), the power input and dissipation do not cancel locally and thus internal stresses tending to distort the domain from circular are present.

When a bias field is applied to a circular domain which is not simply a uniform gradient, the affect of the additional nonuniformities may be taken into account by Fourier decomposition of the z-averaged z component of the applied field at the domain wall with respect to angle. When this is done the constant term determines domain size, the θ term translates the domain, and the $n\theta$ terms, for $n \geqq 2$, deform the domain. The procedure is, of course, only applicable if the domain shape remains near circular.

Coercivity and mobility may be measured either by applying fields to walls[19] and using equation (47) or by applying field gradients to entire cylindrical domains[20] and using equation (61). In the platelets of material which have a coercivity which is so low as to make them useful for device applications it has been found convenient to use a second domain to provide the field gradient for the coercivity measurements. In this measurement two domains are brought together and then released, the coercivity being given by the formula[5]

$$H_c = (4\pi M_s)\frac{3\pi}{8}\frac{r_0^3 h}{s^4} \tag{64}$$

where s is the center-to-center distance of the two circular domains. Equation (64) was obtained using equation (61) and the z component of the dipole field from the second domain at the center of the plate, $2M_s\pi r_0^2 h/s^3$.

3.3 *Domain Size in the Presence of Dissipative Processes* ($n = 0$)

The domain size variation mode Δr_0 has two properties which are not common to the other modes: First, large variations from equilibrium may be considered using the force function, $F(d/h)$, as well as small variations from equilibrium using the radial stability function, $S_0(d/h)$. Second, arbitrary dissipation functions may be considered because the rotational symmetry of the motion removes any tendency for an initially circular domain to couple in other modes.

3.3.1 *Large Variations in Domain Size*

Setting all the $d\Delta r_n/dt$ except $d\Delta r_0/dt$ equal to zero in equation (53) yields the dissipation produced by a domain size change

$$P_{diss} = 4\pi M_s h r_0 \left[\pm H_c + \frac{1}{\mu_w}\frac{d\Delta r_0}{dt}\right]\frac{d\Delta r_0}{dt} \tag{65}$$

where the upper sign is for an expanding domain. Setting the sum of the power dissipation and the rate of energy change from equation (7)

$$\frac{dE_T}{dt} = \frac{dE_T}{d\Delta r_0}\frac{d\Delta r_0}{dt} = 4(2\pi M_s^2)(\pi h^2)\left[\frac{l}{h} + \frac{d}{h}\frac{H}{4\pi M_s} - F\left(\frac{d}{h}\right)\right]\frac{d\Delta r_0}{dt} \quad (66)$$

equal to zero yields the differential equation for the domain diameter $[d\Delta r_0 = dr_0 = \frac{1}{2}d(d)]$

$$-\frac{h}{2\mu_w(4\pi M_s)}\frac{d}{h}\frac{d\left(\frac{d}{h}\right)}{dt} = \frac{l}{h} + \frac{d}{h}\frac{H \pm H_c}{4\pi M_s} - F\left(\frac{d}{h}\right). \quad (67)$$

The domain diameter thus relaxes toward a value which is a solution to the force equation (14) in which the bias field H has been replaced by a composite bias field, $H \pm H_c$. After this substitution is carried out, the equilibrium diameters are obtained as described in Section 2.1 except that the sign of $\pm H_c$ must now be determined in each case and now there is a small continuous range of stable solutions about both the stable and unstable zero coercivity solutions. There are again two solution diameters for each $H \pm H_c$ when $0 < H \pm H_c < H_0$. In the present case, however, coercivity produces two stable ranges of solutions rather than one stable solution point and one unstable solution point. The large diameter solutions to the force equation for $H + H_c$ and $H - H_c$ bound the solution range which brackets the zero coercivity stable solution and similarly the small diameter solutions to the force equation for $H + H_c$ and $H - H_c$ bound the solution range which brackets the zero coercivity unstable solution.

Figure 10 shows the graphical construction for the case $l/h = 0.300$, $H/4\pi M_s = 0.2544$, $H_c/4\pi M_s = 0.020$. The zero coercivity stable and unstable solutions at $d/h = 2.000$ and $d/h = 0.767$ are marked $\mathcal{S}$ and $\mathcal{U}$ respectively; the large diameter solutions for $H + H_c$ and $H - H_c$ at $d/h = 1.527$ and $d/h = 2.468$ are marked $\mathcal{S}_+$ and $\mathcal{S}_-$ respectively and the small diameter solutions for $H + H_c$ and $H - H_c$ at $d/h = 0.919$ and $d/h = 0.685$ are marked $\mathcal{U}_+$ and $\mathcal{U}_-$ respectively. A domain having a diameter greater than that at $\mathcal{S}_-$ will relax toward the diameter at $\mathcal{S}_-$ as indicated by the arrow. Coercivity stabilizes domains having diameters between $\mathcal{S}_+$ and $\mathcal{S}_-$. Domains having diameters between the diameter at $\mathcal{S}_+$ and $\mathcal{U}_+$ will relax toward $\mathcal{S}_+$ as indicated by the arrow. Coercivity stabilizes domains having diameters between $\mathcal{U}_+$ and $\mathcal{U}_-$. Small diameter coercivity stabilized solutions have been observed in the process of carrying out the mobility measurement described in the second paragraph which follows.[7] Domains having diameters smaller

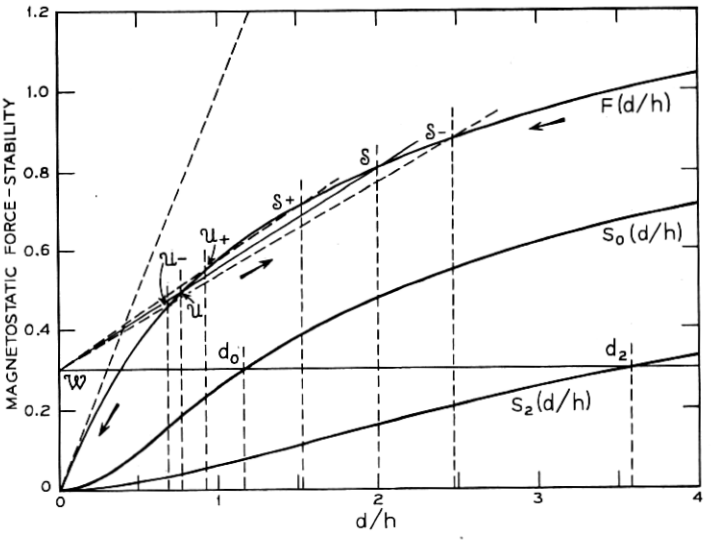

Fig. 10—Construction of solutions to the force equation in the presence of coercivity, $l/h = 0.3$, $H/4\pi M_s = 0.2544$, $H_c/4\pi M_s = 0.020$.

than $\mathfrak{U}_-$ will collapse as indicated by the arrow. The rate of change of domain diameter in any of the dynamic processes described is, of course, given by equation (67).

It can be seen that the collapse diameter is independent of coercivity to the extent that the coercivity is uniform (this is only approximately true at best). A measurement of the collapse diameter, denoted by d_m here, yields the characteristic length

$$l = hS_0(d_m/h) \tag{68}$$

independent of the coercivity. If H_c is then measured from the diameter hysteresis and this value is subtracted from the measured collapse field, the value of $4\pi M_s$ is obtained.

Bobeck[17,18] has developed a method for measuring mobilities which requires only the observation of static domain states. In this method the domain is biased to a stable diameter and then a short duration field pulse having a magnitude, H_P , such that the total field amplitude exceeds the collapse field, $H + H_P > H_0$, is applied. The pulse duration is at first kept so short that at the end of the pulse, the domain has a diameter between the zero coercivity stable and unstable solution so that it recovers its initial size. The pulse length is then gradually

increased until the diameter at the end of the pulse is less than the unstable solution diameter so that the domain collapses.

Figure 11 is a construction illustrating the mobility method for $l/h = 0.30$, $H/4\pi M_s = 0.254$, $H_P/4\pi M_s = 0.246$ and zero coercivity. Under these conditions, $(H + H_P)/4\pi M_s = 0.500 > H_0/4\pi M_s = 0.283$, and the solution diameters are $d_s/h = 2.00 > d_0/h = 1.16 > d_u/h = 0.77$ where d_s is the stable solution diameter and d_u is the unstable solution diameter. In the figure the static collapse point is denoted by $\mathcal{C}$. The domain is initially at the stable equilibrium point $\mathcal{S}$. Application of a fast rise bias field pulse of amplitude H_P takes the domain to $\mathcal{S}'$ where it collapses towards $\mathcal{W}$. If the pulse is turned off at $\mathcal{R}'$ (above the unstable solution point); the diameter increases until the point $\mathcal{S}$ is again reached. If, on the other hand, the pulse has sufficient duration to reach $\mathcal{D}'$ so that the domain state reaches $\mathcal{D}$, the domain collapses to $\mathcal{W}$. In the insert, the field pulse shape used in making the measurement is shown as a function of time.

When the domain velocity is proportional to the applied field and

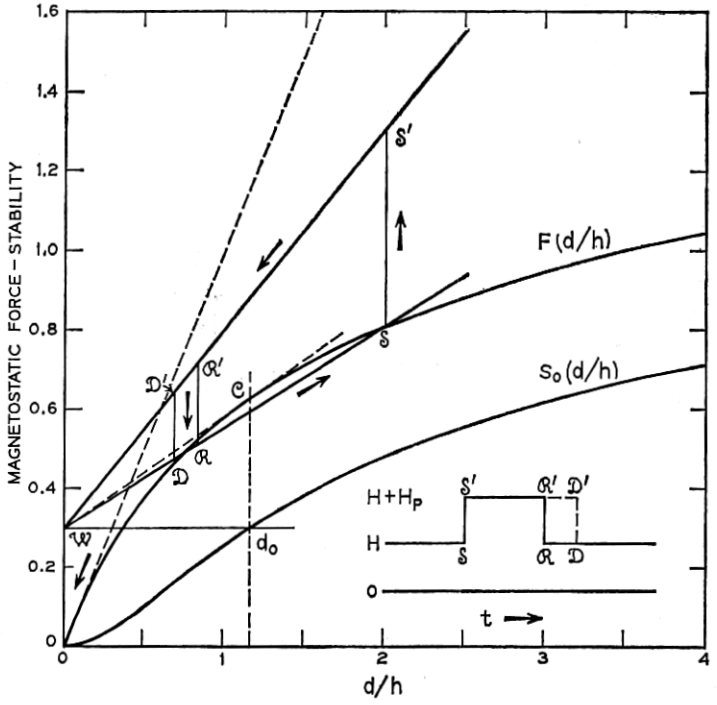

Fig. 11—Construction used in the pulsed bias field mobility method, $l/h = 0.3$, $H/4\pi M_s = 0.254$, $(H + H_P)/4\pi M_s = 0.500$.

pulse rise time effects may be neglected, the mobility is

$$\mu_w = \frac{h}{2T4\pi M_s} \int_{d_u/h}^{d_s/h} \frac{\frac{d}{h}\, d\left(\frac{d}{h}\right)}{\frac{l}{h} + \frac{d}{h}\frac{H}{4\pi M_s} - F\left(\frac{d}{h}\right)} \tag{69}$$

where T is the minimum pulse duration which results in the collapse of the domain. When coercivity must be taken into account the limits of the integral change as described previously. (At the beginning of the pulse the domain is at the point s_+ of Fig. 10.) If additionally nonlinear velocity-drive field relations and pulse rise times must be considered, it is not possible to obtain the mobility as a simple integral over the diameter and the integration is better carried out with respect to time.

3.3.2 *Small Variations in Domain Size from Equilibrium*

This section considers the effect of dissipative processes on domain size for the case where the energy variation expression (7) may be considered an expansion of the energy about the domain diameter which is a solution to the force equation (14). In this case the rate of change of energy with respect to time using (7) is

$$\begin{aligned} \frac{dE_T}{dt} &= \frac{\partial E_T}{\partial \Delta r_0}\frac{d\Delta r_0}{dt} \\ &= -8\pi h(2\pi M_s^2)\frac{h}{d}\left[\frac{l}{h} - S_0\left(\frac{d}{h}\right)\right]\Delta r_0 \frac{d\Delta r_0}{dt}. \end{aligned} \tag{70}$$

Again equating the rate of energy decrease to the power dissipation (65) yields for the linearized differential equation for radial motion

$$\frac{1}{\mu_w(4\pi M_s)}\frac{d\Delta r_0}{dt} = \left(\frac{h}{d}\right)\left[\frac{l}{h} - S_0\left(\frac{d}{h}\right)\right]\frac{\Delta r_0}{r_0} \mp \frac{H_c}{4\pi M_s}. \tag{71}$$

The domain radius thus relaxes towards

$$\frac{|\Delta r_0|}{r_0} = \frac{H_c}{4\pi M_s}\left|\frac{d/h}{l/h - S_0(d/h)}\right| \tag{72}$$

if the domain is stable or, in the case of an unstable domain, coercivity stabilizes the domain for departures in radius from equilibrium up to this same value. In either case, stable or unstable, the relaxation time [defined by the time factor $\exp(-t/\tau)$] is

$$\tau = -\frac{r_0}{\mu_w 4\pi M_s}\frac{d/h}{l/h - S_0(d/h)}. \tag{73}$$

The factor $d/h[l/h - S_0(d/h)]^{-1}$ in equations (71), (72) and (73) is a measure of the radial compliance of the domain relative to coercivity or mobility and will be called the radial relative compliance function. The value of this function may be obtained as the inverse slope of a line constructed on a plot of the force and stability functions. Such a construction is shown in Fig. 12 for $l/h = 0.30$, $d/h = 2.00$, $H/4\pi M_s = 0.2544$. The numerical slope of the line $\mathfrak{W}\mathfrak{R}$ drawn from l/h on the vertical axis to the point on S_0 at $d/h = 2.00$ is 0.0883 so that $d/h[l/h - S_0]^{-1} = 11.33$. Thus, in this case, for a domain to have a diameter defined to within ten percent, the coercivity must be $H_c < 0.01(4\pi M_s)$.

At the collapse diameter, d_0, the relative radial compliance is, of course, infinite while at the other end of the range of stability (the elliptical runout diameter) where in the present example $d_2/h = 0.358$, the relative radial compliance has the value 9.57. The minimum value of the relative radial compliance for $l/h = 0.30$ is 9.52 occurring at a diameter of $d/h = 3.22$. This behavior of the radial relative compliance at $l/h = 0.30$ is typical for thicknesses near the preferred value of $h/l = 4$ as can be seen from Fig. 12. In all such cases, the minimum compliance is achieved at some diameter less than d_2, the compliance being nearly constant from $d = d_2$ down to $(d_0 d_2)^{\frac{1}{2}}$ [for

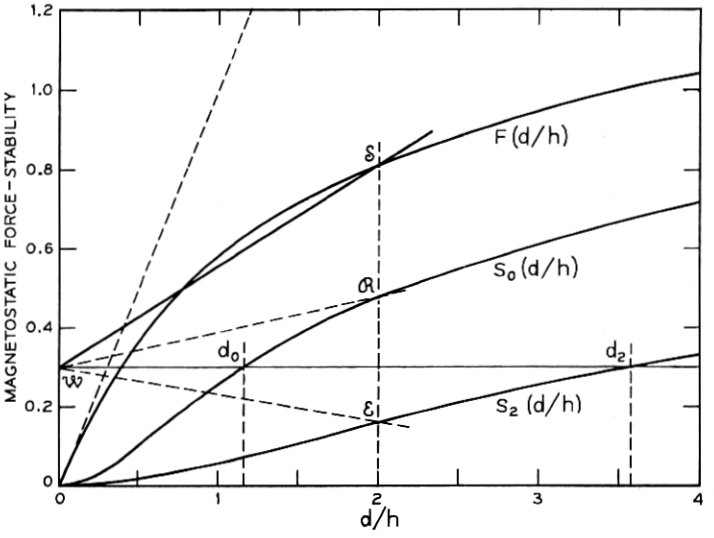

Fig. 12—Construction of the radial and elliptical relative compliance functions for $l/h = 0.3$, $d/h = 2$.

$l/h = 0.30$, $(d_0 d_2)^{\frac{1}{2}}/h = 2.04$] then increasing rapidly to infinity at d_0. The constancy of the radial compliance over a large part of the stable range is related to the linearity of the diameter-field curves away from the collapse diameter [see (36) and Fig. 8].

In Section 3.3.1, the diameters bounding the coercivity stabilized solutions to the equilibrium problem were computed for the case $l/h = 0.30$, $H/4\pi M_s = 0.2544$ and ($d_u/h = 0.767$ $d_s/h = 2.00$ and $H_c/4\pi M_s = 0.020$ using the force equation in the presence of coercivity. As an illustrative consistency check, these bounding diameters will now be computed using the linearized equation (72). The diameters bounding the solution region bracketing the zero coercivity unstable solution obtained from this equation are

$$\frac{d}{h} = \frac{d_u}{h}\left\{1 \pm \frac{H_c}{4\pi M_s}\frac{d_u}{h}\left[\frac{l}{h} - S_0\left(\frac{d_u}{h}\right)\right]^{-1}\right\} = 0.664 \quad \text{and} \quad 0.869,$$

and the diameters bounding the solution region bracketing the zero coercivity stable solution region are

$$\frac{d}{h} = \frac{d_s}{h}\left\{1 \pm \frac{H_c}{4\pi M_s}\frac{d_s}{h}\left[\frac{l}{h} - S_0\left(\frac{d_s}{h}\right)\right]^{-1}\right\} = 1.547 \quad \text{and} \quad 2.453.$$

The corresponding diameters obtained directly from the force equation were $d/h = 0.685$, 0.919, 1.527, and 2.468. The excellent agreement of the diameters bounding the zero coercivity stable solution computed by the two methods is again related to the linearity of the diameter-field curves. Note that the agreement of splittings of the diameters bounding the zero coercivity unstable solution computed the two ways is also quite good.

3.4 *Domain Shape in the Presence of Dissipative Processes* ($n \geq 2$)

The power dissipation produced by the motion of a single mode is from equation (53)

$$P_{\text{diss}} = 4\pi M_s h r_0\left[\pm\frac{2}{\pi}H_c + \frac{1}{2}\frac{1}{\mu_w}\frac{d\Delta r_n}{dt}\right]\frac{d\Delta r_n}{dt}, \qquad n \geq 2, \tag{74}$$

where the upper sign is for positive $d\Delta r_n/dt$. The rate of change of domain energy under these conditions is from (7)

$$\frac{dE_T}{dt} = \frac{\partial E_T}{\partial \Delta r_n}\frac{\partial \Delta r_n}{dt}$$

$$= 4\pi h(2\pi M_s^2)(n^2 - 1)\left(\frac{h}{d}\right)\left[\frac{l}{h} - S_n\left(\frac{d}{h}\right)\right]\Delta r_n \frac{d\Delta r_n}{dt}, \qquad n \geq 2. \tag{75}$$

Setting the sum of the rate of change of the energy and the power dissipation equal to zero yields the differential equation for the relaxation of the variation of a single Δr_n,

$$\frac{1}{\mu_w 4\pi M_s}\frac{d\Delta r_n}{dt} = -(n^2 - 1)\left(\frac{h}{d}\right)\left[\frac{l}{h} - S_n\left(\frac{d}{h}\right)\right]\frac{\Delta r_n}{r_0} \pm \frac{4}{\pi}\frac{H_c}{4\pi M_s}. \qquad (76)$$

The domain shape variation amplitude thus relaxes towards

$$\frac{|\Delta r_n|}{r_0} = \frac{H_c}{4\pi M_s}\left|\frac{4}{\pi}\frac{1}{(n^2 - 1)}\frac{d/h}{[l/h - S_n(d/h)]}\right|, \qquad n \geqq 2, \qquad (77)$$

if the variation is stable or, in the case of an unstable domain, coercivity stabilizes the domain for variations in amplitude up to this same value. In either case, stable or unstable, the relaxation time (defined by the time factor $\exp(-t/\tau)$) is

$$\tau = \frac{r_0}{\mu_w 4\pi M_s}\frac{1}{(n^2 - 1)}\frac{d/h}{[l/h - S_n(d/h)]}, \qquad n \geqq 2. \qquad (78)$$

Whenever the coercivity is effectively zero so that the mobility characterizes all dissipative processes, the normal modes of the domain remain decoupled (within the small amplitude approximation). Each of these modes relaxes according to equations (71) or (76). When coercivity must be considered, these equations become rather crude approximations because even perfectly uniform coercivity introduces nonlinear mode coupling. The nonlinear mode coupling is especially noticeable at the end of the relaxation of a single mode. The reason for phrasing the discussion of the effects of dissipative processes in terms of dissipation equations was to account correctly for the effects of coercivity to lowest order without being required to examine the coupling of the modes or the origins of coercivity. The results obtained do provide a general picture of the dependence of the effect of coercivity on the various domain parameters and in particular they provide a measure of the dependence of the stiffness of the domains on these parameters.

Equations (77) and (78) show that the entire n dependence of the residual distortion of a domain recovering from a fluctuation of a single mode and the relaxation time with which it recovers is contained in the stiffness factor $(n^2 - 1)[l/h - S_n(d/h)]$. The domain stability condition, $S_0 \geqq l/h \geqq S_2$, and the inequality (18) imply that $[l/h - S_n]$ is a monotonic increasing function of n. Therefore the residual Δr_n and relaxation time both decrease slightly faster than $1/n^2$ (see Ref. 1).

Thus, to characterize the effect of coercivity in limiting the attainment of stable movable cylindrical domains it is necessary only to consider the elliptical shape variation mode ($n = 2$) in addition to the size ($n = 0$) and translation ($n = 1$) modes discussed previously.

The factor $(4/3\pi)(d/h)[l/h - S_2(d/h)]^{-1}$ in equations (76), and (77) and (78) for $n = 2$ is a measure of the elliptical compliance of the domain relative to coercivity of mobility and will be called the elliptical relative compliance function. The value of this function is proportional to the inverse slope of a line constructed on a plot of the force and stability functions. Figure 12 shows such a construction for $l/h = 0.30$, $d/h = 2.00$, $H/4\pi M_s = 0.2544$. The numerical slope of the line $\mathfrak{W}\mathfrak{E}$ drawn from l/h on the vertical axis to the point on S_2 at $d/h = 2.00$ is -0.068 so that $(4/3\pi)(d/h)[l/h - S_2]^{-1} = 6.25$. Thus a coercivity less than that value which defines the domain diameter to within ten percent ($H_c < 0.01(4\pi M_s)$) defines the ratio of the difference in the ellipse semiaxes to their average ($2\Delta r_2/r_0$) to 12 percent.

At the elliptical runout diameter, d_2, the relative elliptical compliance is, of course, infinite while at the other end of the range of stability (the collapse diameter) where in the present case $d_0/h = 1.16$ the relative elliptical compliance has the value 2.22. The figure shows that this behavior is true for any value of l/h. In general the minimum value of the relative elliptical compliance occurs at the collapse diameter, the compliance increasing from the minimum in a regular fashion to infinity at the elliptical runout diameter. This regular behavior is in contrast to the behavior of the relative radial compliance.

3.5 *Restrictions Placed on the Region of Device Operation by Consideration of Dissipative Effects.*

The relative compliance functions appearing as factors in equations (72), (73), (77) and (78) contain the dependence of both the normalized residual distortion $\Delta r_n/r_0$, and the normalized relaxation time $\tau(\mu_w 4\pi M_s)/r_0$, upon n, l, h, and d, or H. Although the discussion which follows is phrased in terms of the residual $\Delta r_n/r_0$, it should be kept in mind that the same remarks apply to the relaxation times scaled to $r_0/(\mu_w 4\pi M_s)$, the time required to propagate the domain one radius when the maximum field difference across the domain, ΔH, is $8\pi M_s$ [equation (61)].

In preceding subsections, the following has been demonstrated: Except in the immediate neighborhood of the collapse diameter, the domain diameter and bias field are, within the range of stability,

approximately linearly related (Fig. 8). In the neighborhood of the plate thickness previously termed preferred, $h_p = 4l$ [equation (31)], the radial compliance, considered as a function of the bias field, is roughly constant from $d = (d_0 d_2)^{\frac{1}{2}}$ to $d = d_2$, and at $d = (d_0 d_2)^{\frac{1}{2}}$, the elliptical compliance is one half the radial compliance so that $d = (d_0 d_2)^{\frac{1}{2}}$ represents a reasonable bias condition. Since for $h/l \approx 4$ or in general for any plate thickness, the diameter and bias field ranges are relatively narrow (Fig. 5) the radial and elliptical compliance of domains suitable for device application may be completely characterized with respect to plate thickness by plotting the relative compliance functions with respect to h/l for the bias condition $d = (d_0 d_2)^{\frac{1}{2}}$.

The relative radial compliance,

$$\frac{\Delta r_0/r_0}{H_c/4\pi M_s} = \frac{d/h}{S_0(d/h) - l/h}, \tag{79a}$$

$$\approx 1.085(h/l)^{\frac{1}{2}}, \qquad h/l \gg 1, \tag{79b}$$

$$\approx 3.783 \exp(\pi l/h), \qquad h/l \ll 1, \tag{79c}$$

and the relative elliptical compliance,

$$\frac{\Delta r_2/r_0}{H_c/4\pi M_s} = -\frac{4}{3\pi} \frac{d/h}{S_2(d/h) - l/h}, \tag{80a}$$

$$\approx 1.382(h/l)^{\frac{1}{2}}, \qquad h/l \gg 1, \tag{80b}$$

$$\approx 1.606 \exp(\pi l/h), \qquad h/l \ll 1, \tag{80c}$$

are plotted in Fig. 13 as functions of h/l for the bias condition $d = (d_0 d_2)^{\frac{1}{2}}$. The function values and asymptotic forms were obtained by methods which were used in Section 2.3 to obtain the diameter and field functions. The feature which distinguishes the relative compliance functions from the diameter and field functions is that the diameter and field functions bound the region of domain stability whereas the relative compliance functions provide a measure of the magnitude of the stability of the domains within the stable region.

The constructions of the radial and elliptical relative compliance functions shown in Fig. 12 and described in Sections 3.3.2 and 3.4 for $h/l = 3.33$, $d/h = 2.00$ may be taken as approximate construction for the values of these functions at $h/l = 3.33$ since $(d_0 d_2)^{\frac{1}{2}}/h = 2.04$.

The minimum value of the radial compliance [$d = (d_0 d_2)^{\frac{1}{2}}$] is ≈ 7.9 occurring at a thickness of $h/l \approx 10.3$ and the minimum value of the elliptical compliance [$d = (d_0 d_2)^{\frac{1}{2}}$] is ≈ 5.9 occurring at a thickness

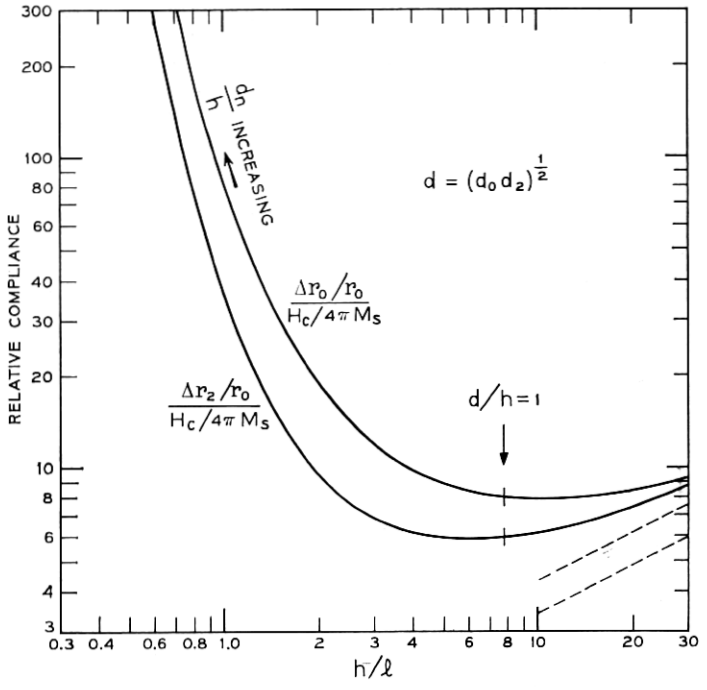

Fig. 13—Radial and elliptical relative compliance functions as a function of the thickness, h, measured in units of the characteristic length, l, for the bias condition $d = (d_0 d_2)^{\frac{1}{2}}$.

of $h/l \approx 6.1$.The compliance minima occur at somewhat greater plate thicknesses than the diameter minima. However, since the functions are quite flat bottomed, they increase only slightly in value from their minima to the thickness value previously termed preferred, $h/l = 4.0$ [equation (31)]. {At $h/l = 4.0$, $(d_0 d_2)^{\frac{1}{2}}/l \approx 6.8$. However, the preferred values were taken to be $h_p = 4l$ [equation (31)], $d_p = 8l$ [equation (32)] so that $d_p/h_p = 2.0$. The exact preferred values depend on the device structure in which the domain is located.}

As in the example of Sections 3.3.2 and 3.4, the coercivity requirement

$$H_c < 0.01(4\pi M_s) \tag{81}$$

will insure that a domain having the preferred thickness and diameter values will show radius function variations from the equilibrium radius of no more than ten percent. Just below $h/l = 4.0$, the increase

in the compliance functions is seen to become exponential so that the observation of stable moveable cylindrical domains in reasonably thin plates is experimentally unlikely. Since the relative compliance functions increase slowly with thickness for thick plates, cylindrical domains may be observed well into the region in which the assumption of cylindrical walls becomes dubious (see Ref. 1, Section 6.1).

Although domains may be observed in thick plates, other considerations cause the realizable bit rate to decrease at least inversely with increasing thickness. These effects are as follows: The ΔH appearing in the domain velocity expression (61) is twice the $n = 1$ Fourier component of the z-averaged z component of the applied field. Since the field gradient is applied from the surface of the plate and obeys Laplace's equation, the variation in the applied field intensity decreases exponentially into the plate from its value at the surface. Thus for a given field variation intensity at the plate surface, the z-averaged z component of the intensity variation decreases inversely with increasing h/d for $h/d > 1$. Now for $d = (d_0\, d_2)^{\frac{1}{2}}$, $d/h = 1$ occurs at $h/l \approx 8$ (see Figs. 2 or 13) and above this value $d/h \approx 2.17(h/l)^{-\frac{1}{2}}$ [see Fig. 4 and equations (23b) and (24b)] so that for thicknesses greater than $h/l \approx 8$, the mobility with respect to the field gradient at the surface of the plate decreases according to $(h/l)^{-\frac{1}{2}}$. Since in a given material the absolute domain diameter increases with increasing plate thickness in this region according to $d/l \approx 2.17(h/l)^{\frac{1}{2}}$, the bit-rate decreases according to $(h/l)^{-1}$. If additionally the maximum field difference at the surface of the plate is assumed to be some fraction of the difference of the collapse and runout fields, $H_0 - H_2$, then it is seen from equations (27b), (28b) and (30b) that the bit-rate decreases according to $(h/l)^{-\frac{3}{2}}$.

Thus in summary, consideration of the effects of dissipative processes even more strongly defines the neighborhood of $h_p/l = 4$, $d_p/l = 8$ as the preferred region than did considerations of stability only and additionally yields the requirement $H_c/4\pi M_s < 0.01$ for the attainment of stable movable domains.

IV. DETERMINATION OF MATERIAL PARAMETERS FROM PREFERRED DEVICE PARAMETERS*

The preceding sections have provided preferred values of the plate thickness (31) and domain diameter (32) or bias field, and the least

* Reference 21 includes part of the material of this section in a discussion of the relation of the M_s and K_u values of materials (available at that time) to the preferred values of these parameters.

permissible value of the anisotropy constant (1). Additionally it was shown that the wall mobility acts to form the scale factor for time. For device construction it is desirable to specify the domain diameter, d_p, from considerations of bit density and the resolution of mask-making and etching procedures while maximizing the bit rate. Once the domain diameter is specified, the desired characteristic material length is determined by equation (32) as $l \approx d_p/8$, the thickness is determined by equation (31) as $h_p \approx \frac{1}{2}d_p$, and the applied field is specified by equation (14) as $H \approx 0.28(4\pi M_s)$. It will now be shown that by adding assumptions about mobility and room temperature operation to conditions (1) and (31), it is possible to specify uniquely the three parameters A, K_u and M_s appearing in the energy density expression for the simplest uniaxial material[22]

$$\rho_E = A\left[\left(\frac{\partial\theta}{\partial s}\right)^2 + \sin^2\theta\left(\frac{\partial\phi}{\partial s}\right)^2\right] + K_u \sin^2\theta - \mathbf{H}_L\cdot\mathbf{M}. \tag{82}$$

In equation (82), A is the isotropic exchange constant, θ is the polar angle (the angle between the magnetization and the z axis), ϕ is the azimuthal angle, s is the distance through the wall, K_u is the uniaxial anisotropy constant, $\mathbf{M}$ is the magnetization vector ($|\mathbf{M}| = M_s$) and $\mathbf{H}_L$ is the sum of the applied and demagnetizing fields. Only Bloch walls in this simplest uniaxial material will be considered. Achievement of the coercivity condition (81) is a function of both intrinsic material properties and processing and will not be considered here.

In Section VI of Ref. 1, it was shown that from several standpoints

$$q \equiv K_u/2\pi M_s^2, \tag{83}$$

the dimensionless ratio of the uniaxial anisotropy constant to the energy density of a volume containing a magnetic field of strength $4\pi M_s$ must at least be greater than one, equation (1). From the definitions of q, l, and d_p and the expressions for the Bloch wall width and energy in the simplest uniaxial material (82), $l_w = \pi(A/K_u)^{\frac{1}{2}}$ and $\sigma_w = 4(AK_u)^{\frac{1}{2}}$,[22] the ratio of preferred domain diameter to the wall width is

$$\frac{d_p}{l_w} = \frac{16}{\pi}\, q. \tag{84}$$

If q were much less than one then the domain wall width would be larger than the domain diameter and clearly no domain of the type which has been considered here could exist. On the other hand, if q is very large the domain wall is very narrow with respect to the domain

diameter. For a given rate of flipping over of the spin systems comprising the wall, the bit-rate will thus be inversely proportional to q. It may thus be expected that everything else being equal (it is not clear at the present time just exactly what is to be held constant) that materials with high q values will have low bit-rates in devices whose speed is drive field limited. A q value of approximately three may thus be termed preferred.

The range of values of the exchange constant, A, occurring in materials which may be considered for room temperature device applications is quite limited as can be seen from the following argument: For a given structure and density of spin systems, the exchange constant is expected to be proportional to the Curie or Néel temperature, T_n.[23] For room temperature device applications, as a practical matter, T_n must be above approximately 400°K. Since the highest observed T_n are approximately 1000°K, the range of allowable T_n and therefore the range of A in acceptable materials is nearly determined.

F. B. Hagedorn, D. H. Smith, and F. C. Rossol have combined domain measurements of l with magnetometer measurements of K_u and $4\pi M_s$ to obtain the exchange constant in two materials.[24] They find for $Sm_xTb_{1-x}FeO_3$ ($x \approx 0.55$, $T_n = 661$°K), $A = 0.4 \times 10^{-6}$ ergs per cm and for $PbFe_{12-x}Al_xO_{19}$ ($x \approx 4.0$, $T_n = 508$°K) $A = 0.1 \times 10^{-6}$ ergs per cm, values which are apparently typical for high T_n iron oxides.

Since the exchange constant, A, is to be considered fixed, q has the preferred value three and d has the preferred value d_p, it is appropriate to solve for the magnetization and anisotropy constant in terms of these quantities,

$$4\pi M_s = 32(2\pi qA)^{\frac{1}{2}}/d_p \tag{85}$$

and

$$K_u = 256Aq^2/d_p^2 . \tag{86}$$

If $A = 4.0 \times 10^{-7}$ ergs per cm, $q = 3$ and $d_p = 10^{-3}$ cm (approximately one mil bit spacing) then $4\pi M_s \approx 80$ Gauss and $K_u \approx 900$ ergs per cc which are both numerically small.

Maintaining the values of A and d_p but considering q as variable (85) becomes $4\pi M_s \approx 50\sqrt{q}$. Thus q any within two orders of magnitude of the preferred value produces a value of $4\pi M_s$ of one kilogauss or smaller. Since the magnetic moment per spin system and the volume of the individual spin systems are approximately constants and since

the exchange interaction is of short range, low saturation magnetizations cannot be achieved by dilution of the spin systems with magnetically unordered materials. Spin system density thus must be high while the net magnetic moment per unit volume remains low. Some sort of antiferromagnetic character is thus required in magnetic materials which are candidates for use in cylindrical domain devices. Typical systems are ferrimagnets, and canted antiferromagnets.

The K_u value of 900 ergs per cc is quite low for a symmetry allowed intrinsic uniaxial anisotropy constant.[21] When low anisotropies are obtained by operating near the reorientation temperature in canted systems[25] or near the Neel temperature, the material parameters tend to be undesirably temperature dependent. Since uniaxial anisotropy energy densities of the required value may be induced, it appears that the use of materials having induced anisotropy, such as the recently announced garnets,[17,18,26] appears quite promising.

Having determined that A is to be considered fixed and that K_u and M_s have preferred values, this section concludes by showing the dependence of several overall device parameters on these parameters and the mobility. The device parameters considered are the bit density, bit rate, the domain flux which is important in Hall effect detectors[27] and the induced voltage which is important in wire pickup loop detectors.

In typical domain devices, the bit positions form a square array with the bit spacing being three to four domain diameters (see figures of References 4 and 5). If the bit spacing is assumed to be $3d_p$, then the number of bit locations per square centimeter is

$$\rho_b = (3d_p)^{-2} = 6.9 \times 10^{-7}(4\pi M_s)^4/AK_u . \tag{87}$$

Since the bit density is such a strong function of $4\pi M_s$ the magnetization is nearly determined once a bit density is specified.

The difference of the collapse and runout bias field for a plate of the preferred thickness $h = 4l$ is $H_0 - H_2 \approx 0.1\ (4\pi M_s)$. Retaining the assumption of a bit spacing of $3d_p$ and assuming that the device structure continuously maintains a field difference across the domain of $0.1(4\pi M_s)$ the bit rate in bits per second is

$$f_b = v_b/3d_p = \mu_w 4\pi M_s/60d_p = 4.1 \times 10^{-5}\mu_w(4\pi M_s)^3(AK_u)^{-\frac{1}{2}}, \tag{88}$$

linear in the mobility and again dominated by the $4\pi M_s$ dependence of d_p. If it is assumed that a pickup loop intercepts one half of the flux emerging from the magnetic charges forming the upper surface

of the cylindrical domain, then the flux change produced by moving a cylindrical domain under the loop in gauss square centimeters is

$$\Phi = \frac{\pi}{8} d_p^2(4\pi M_s) = 6.4 \times 10^4 AK_u(4\pi M_s)^{-3}. \tag{89}$$

If it is assumed that this flux change takes place in the time required for a domain driven by a field difference of $0.1(4\pi M_s)$ to propagate a distance d_p, the induced (MKS practical) voltage is

$$V = \frac{\pi}{160} \mu_w(4\pi M_s)^2 d_p \times 10^{-8} = 7.9 \times 10^{-8} \mu_w(AK_u)^{\frac{1}{2}}. \tag{90}$$

V. ACKNOWLEDGMENTS

The author wishes to acknowledge H. E. D. Scovil for his encouragement to complete this work, A. W. Anderson and F. B. Hagedorn for reading the manuscript and making comments, P. I. Bonyhard for initially demonstrating the usefulness of graphical methods for obtaining the properties of the solutions to the force equation and A. H. Bobeck, whose experiments provided much of the motivational basis for this work.

REFERENCES

1. Thiele, A. A., "The Theory of Cylindrical Magnetic Domains," B.S.T.J., *48*, No. 10 (December, 1969), pp. 3287–3335.
2. Thiele, A. A., "Theory of the Static Stability of Cylindrical Domains in Uniaxial Platelets," J. Appl. Phys., *41*, No. 3 (March, 1970), pp. 1139–1145.
3. Kooy, C., and Enz, U., "Experimental and Theoretical Study of the Domain Configuration in Thin Layers of $BaFe_{12}O_{19}$," Philips Res. Rep., *15*, No. 1 (February, 1960), pp. 7–29.
4. Bobeck, A. H., "Properties and Device Applications of Magnetic Domains in Orthoferrites," B.S.T.J., *46*, No. 8 (October, 1967), pp. 1901–1925.
5. Bobeck, A. H., Fischer, R. F., Perneski, A. J., Remeika, J. P., and Van Uitert, L. G., "Application of Orthoferrites to Domain-Wall Devices," IEEE Trans. Magnetics, *5*, No. 3 (September, 1969), pp. 544–553.
6. Perneski, A. J., "Propagation of Cylindrical Magnetic Domains in Orthoferrites," IEEE Trans. Magnetics, *5*, No. 3 (September, 1969), pp. 554–557.
7. Bobeck, A. H., unpublished work.
8. Bobeck, A. H., and Sherwood, R. C., unpublished work.
9. Della Torre, E., and Dimyan, M. Y., "Anisotropy of Wall Energy in Orthoferrites," IEEE Trans. Magnetics *MAG-6*, No. 3 (September 1970), pp. 489–492.
10. Hagedorn, F. B., Tabor, W. J., and Thiele, A. A., unpublished work.
11. Shumate, P. W., unpublished work.
12. Galt, J. K., "Motion of a Ferromagnetic Domain Wall in Fe_3O_4," Phys. Rev., *85*, No. 4 (February, 1952), pp. 664–669.
13. Galt, J. K., "Motion of Individual Domain Walls in a Nickel-Iron Ferrite," B.S.T.J., *33*, No. 5 (September, 1954), pp. 1023–1054.
14. Dillon, J. F., Jr., and Earl, H. E., Jr., "Domain Wall Motion and Ferromag-

netic Resonance in a Maganese Ferrite," J. Appl. Phys., *30,* No. 2 (February, 1959), pp. 202–213.
15. Asti, G., Colombo, M., Giudici, M., and Levialdi, A., "Magnetization Dynamics in $BaO \cdot 6Fe_2O_3$ Single Crystals Using Pulsed Magnetic Fields," J. Appl. Phys., *36,* No. 11 (November, 1965), pp. 3581–3585.
16. Asti, G., Colombo, M., Giudici, M., and Levialdi, A., "Domain-Wall Motion in Barium Ferrite Single Crystals," J. Appl. Phys., *38,* No. 5 (April, 1967), pp. 2195–2198.
17. Bobeck, A. H., "A Second Look at Magnetic Bubbles," talk given at the Int. Magnetics Conf., Washington, D. C., April 21–24, 1970.
18. Bobeck, A. H., Danylchuk, I., Remeika, J. P., Van Uitert, L. G., and Walters, E. M., "Dynamic Properties of Bubble Domains," talk given at the Int. Conf. Ferrites, Kyoto, Japan, July 6–9, 1970.
19. Rossol, F. C., "Domain-Wall Mobility in Rare-Earth Orthoferrites by Direct Stroboscopic Observation of Moving Domain Walls," J. Appl. Phys., *40,* No. 3 (March, 1969), pp. 1082–1083.
20. Rossol, F. C., and Thiele, A. A., "Domain Wall Dynamics Measured Using Cylindrical Domains," J. Appl. Phys., *41,* No. 3 (March, 1970), pp. 1163–1164.
21. Gianola, U. F., Smith, D. H., Thiele, A. A., and Van Uitert, L. G., "Material Requirements for Circular Magnetic Domain Devices," IEEE Trans. Magnetics, *5,* No. 3 (September, 1969), pp. 558–561.
22. Chikazumi, S., *Physics of Magnetism,* New York: John Wiley and Sons, Inc., 1964, Chap. 9.
23. Weiss, P. R., "The Application of the Bethe-Peierls Method to Ferromagnetism," Phys. Rev., *74,* No. 10 (November, 1948), pp. 1493–1504.
24. Hagedorn, F. B., Rossol, F. C., and Smith, D. H., unpublished work.
25. Rossol, F. C., "Temperature Dependence of Rare-Earth Orthoferrite Properties Relevant to Propagating Domain Device Applications," IEEE Trans. Magnetics, *5,* No. 3 (September, 1969), pp. 562–565.
26. Bobeck, A. H., Spencer, E. G., Van Uitert, L. G., Abrahams, S., Barns, R., Grodkiewicz, W. H., Sherwood, Schmidt, P., Smith, D. H., and Walters, E. M., "Uniaxial Magnetic Garnets for Domain Wall Bubble Devices," Appl. Phys. Letters, *17,* No. 3 (August 1970), pp. 131–134.
27. Strauss, W., and Smith, G. E., "Hall-Effect Domain Detector," J. Appl. Phys., *41,* No. 3 (March, 1970), pp. 1169–1170.